HHS Public Access

Author manuscript

J Immunol. Author manuscript; available in PMC 2019 January 15.

Published in final edited form as:

J Immunol. 2018 January 15; 200(2): 483–499. doi:10.4049/jimmunol.1601793.

Role of the EHD family of endocytic recycling regulators for TCR recycling and T-cell function

Fany M. Iseka[*,†], **Benjamin T. Goetz**[*], **Insha Mushtaq**[*,§], **Wei An**[*], **Luke R. Cypher**[*], **Timothy A. Bielecki**[*], **Eric C. Tom**[*,‡], **Priyanka Arya**[*,†,#], **Sohinee Bhattacharyya**[*,§,**], **Matthew D. Storck**[*], **Craig L. Semerad**[††], **James E. Talmadge**[§], **R. Lee Moseley**[*,¶], **Vimla Band**[*,†,§], and **Hamid Band**[*,†,‡,§,¶]

[*]Eppley Institute for Research in Cancer and Allied Diseases; University of Nebraska Medical Center, Omaha, NE 68198, U.S.A

[†]Departments of Genetics, Cell Biology & Anatomy, University of Nebraska Medical Center, Omaha, NE 68198, U.S.A

[§]Pathology & Microbiology, University of Nebraska Medical Center, Omaha, NE 68198, U.S.A

[‡]Biochemistry & Molecular Biology, University of Nebraska Medical Center, Omaha, NE 68198, U.S.A.; and Pharmacology & Experimental Neuroscience, University of Nebraska Medical Center, Omaha, NE 68198, U.S.A

[¶]Fred & Pamela Buffet Cancer Center, University of Nebraska Medical Center, Omaha, NE 68198, U.S.A

[††]Flow Cytometry Research Facility, University of Nebraska Medical Center, Omaha, 68198, U.S.A

Abstract

T cells use the endocytic pathway for key cell biological functions, including receptor turnover and maintenance of the immunological synapse. Some of the established players include the Rab GTPases, the SNARE complex proteins and others, which function together with Eps15 Homology Domain-containing (EHD) proteins in non-T-cell systems. To date, the role of the EHD protein family in T-cell function remains unexplored. We generated conditional EHD1/3/4 knockout mice using CD4-Cre and crossed these with mice bearing a myelin oligodendrocyte glycoprotein (MOG)-specific TCR transgene. We found that $CD4^+$ T-cells from these mice exhibited reduced antigen-driven proliferation and IL-2 secretion *in vitro*. *In vivo*, these mice exhibited reduced severity of experimental autoimmune encephalomyelitis. Further analyses showed that recycling of the TCR-CD3 complex was impaired, leading to increased lysosomal targeting and reduced surface levels on $CD4^+$ T cells of EHD1/3/4 knockout mice. Our studies

Corresponding Author: Hamid Band, M.D., Ph.D. Eppley Institute for Research in Cancer and Allied Diseases, BCC 10.12.390, 986805 Nebraska Medical Center, Omaha, NE 68198-6805. hband@unmc.edu. Phone: 402-559-8572; Fax: 402-559-4651.

[#]**Current Address:** Priyanka Arya - Department of Medical and Molecular Genetics, Indiana University School of Medicine, Indianapolis, IN, 46202; U.S.A.

[**]**Current Address:** Sohinee Bhattacharyya - Department of Cell, Developmental & Cancer Biology, Oregon Health Science University, Portland, OR 97239; U.S.A.

DISCLOSURES:

The authors declare no financial conflicts of interest.

reveal a novel role of the EHD family of endocytic recycling regulatory proteins in TCR-mediated T-cell functions.

INTRODUCTION

Understanding of the mechanisms that underlie proper T-cell function is of great interest in basic immunology and immunopathology. T-cell activation requires recognition of an antigenic peptide bound to MHC proteins on antigen presenting cells (APC) by the T-cell antigen receptor (TCR) and downstream signaling mediated by cytoplasmic regions of the TCR-CD3 complex. Effective generation of an immune response requires concurrent engagement of and signaling through co-stimulatory proteins (e.g., CD28) on T-cells by their cognate ligands on the APC surface (1). Therefore, the mechanisms that ensure optimal levels of the TCR and accessory receptors on the T-cell surface prior to antigen stimulation are fundamentally critical to generating an effective immune response. However, mechanisms that regulate the surface pool of TCR and its accessory receptors have been primarily investigated in the context of T-cell activation. During T-cell activation, TCR signaling elicited by the APC-presented antigen, together with co-stimulatory signals, leads to spatial reorganization of the TCR and accessory receptors, such as CD28 and lymphocyte function-associated 1 (LFA-1), to form an area of intimate contact with APCs, the immunological synapse (IS) (2, 3). The endocytic pathways supply the IS with newly-synthesized and recycled receptors to replenish those that are targeted to the lysosome for degradation (4–6).

Cells use clathrin-dependent as well as clathrin-independent pathways to internalize surface receptors into early endosome (EE)/sorting endosome compartments, from where they traffic to late endosome/multi-vesicular bodies and lysosomes for degradation, or recycle back to the cell surface either through a $Rab4^+$ fast recycling endosome (RE) (directly to the plasma membrane) or through a slow recycling route via the $Rab11^+$ RE (7, 8). This sorting processes is known to be regulated by Rab family of small GTPases and their interacting partners (9). T-cell receptors such as TCR-CD3 (1), CD28 (10) and LFA-1 (11, 12) are known to be internalized and recycled to the IS during T-cell activation. Internalized TCR-CD3 traverses the $Rab5^+$ EE, followed by transport through $Rab4^+$ and $Rab11^+$ endosomes, indicating the involvement of both fast and slow recycling pathways (13, 14). Naïve and resting T-cells constitutively internalize and recycle their surface receptors and the balance of these processes dictates their pre-stimulation surface levels and hence the levels of T-cell activation (13). Yet, the mechanisms of constitutive basal traffic of TCR-CD3 are not fully understood.

Recently, a new family of endocytic regulators, the EPS15 Homology Domain-containing proteins (EHD1-4), has been identified. These proteins exhibit a conserved domain architecture with helical regions near the N-terminus and the middle of the protein surrounding an ATP-binding G-domain that can hydrolyze ATP slowly, and a C-terminal EH domain that binds to proteins with asparagine-proline-phenylalanine (NPF)-containing or related tripeptide motifs as a major mechanism of protein-protein interactions (15, 16). Structural studies of EHD2 reveal that the helical regions form a curved membrane lipid-

binding interface, and that the ATPase domain folds like the GTPase domain of dynamin and mediates the formation of stable dimers (17). Other structural findings support a model that dimeric EHDs organize into oligomeric rings around curved membrane structures and function in membrane tubulation and vesiculation (17–21). Consistent with these biochemical observations, cell biological studies have shown that EHD proteins regulate recycling of several surface receptors that traffic through clathrin-dependent or clathrin-independent pathways, including transferrin receptor, MHC class I, β1 integrin, AMPA receptors, insulin-like growth factor 1 receptor (IGF1R), insulin-responsive glucose transporter 4 (GLUT4), and others (7, 22–29). However, the physiological relevance of the many *in vitro* assigned roles of EHD proteins remains to be defined.

We used gene targeting in mice to reveal the *in vivo* functional roles of EHD proteins and cell surface receptors whose traffic is regulated by EHDs (30–36). For example, EHD1 KO mice exhibit strain-dependent phenotypes varying degrees of embryonic lethality, male infertility, ocular developmental defects, and neural tube closure defects due to impairment of ciliogenesis and SHH signaling (37, 38).

To date, any roles of EHD-family proteins in TCR traffic or T-cell function are unknown. Given their importance in the regulation of a variety of other cell surface receptors and the consequences of deleting their genes, singly or in combination, on organ/cell function *in vivo*, we hypothesized that EHD proteins could play an important functional role in T cells by regulating receptor traffic. Consistent with such a hypothesis, EHD proteins have been shown to interact with Rab effectors, such as Rabenosyn-5, a dual Rab4 and Rab5 effector in the early endosome (39), and Rab11 effector, Rab11-FIP2, which regulates the exit of vesicles from the recycling endosome back to the plasma membrane (40). Moreover, EHD proteins (EHD1, EHD3, and EHD4) were shown to interact with SNARE complex proteins such as SNAP-25, SNAP29 (41, 42), Syndapin I and II (7, 43, 44), and other proteins in non-T-cell systems. EHD proteins have been shown to localize in endosomes positive for Rab5, Rab4, Rab8, Rab11 or Rab35 (9, 25, 29, 45), compartments that ae implicated in TCR traffic (46–48). Thus, we posited that EHD proteins could play an important functional role in T-cells.

We found that EHD 1, 3 and 4 are expressed in lymphoid tissues and in purified $CD4^+$ T-cells. Accordingly, we generated myelin oligodendrocyte glycoprotein (MOG)-specific TCR transgene (2D2-TCR Tg)-bearing mice in which floxed EHD 1, 3 and 4 were deleted using a CD4-Cre transgene. *In vitro*, $CD4^+$ T-cells of *EHD1*$^{fl/fl}$*; EHD3*$^{fl/fl}$*; EHD4*$^{fl/fl}$*; Cd4-cre; 2D2Tcr* mice (EHD1/3/4 knockout) exhibit reduced antigen-driven cell proliferation and IL-2 secretion. *In vivo*, these mice exhibit a reduced severity of experimental autoimmune encephalomyelitis (EAE) elicited by immunization with the MOG peptide. We show that surface levels of TCR, CD28, and LFA-1 are reduced and TCR recycling is impaired in $CD4^+$ T-cells of mice with a CD4-Cre mediated EHD1/3/4 knockout. Therefore, our studies reveal a novel role of the EHD family of endocytic recycling proteins in the surface display of TCR in unstimulated T-cells that contributes to their positive functional role in antigen-induced T-cell activation and immunopathology.

MATERIALS AND METHODS

Reagents & Antibodies

Reagents—BSA (cat. # A7906-100G), paraformaldehyde (cat. # 158127-500G), Triton X-100 (cat. # 93418), EGTA (cat # E8145-50G), sodium orthovanadate (Na_3VO_4, cat # S6508-50G), sodium deoxycholate (cat # D6750-100G), 4-hydroxtamoxifen (cat. # T176-10MG), and Brefeldin A (BFA, cat**. #** B7651) were from Sigma-Aldrich (St. Louis, MO). Propidium iodide staining solution (cat. # 00-6990-42) was from eBiosciences. ^{3}H-thymidine (cat. # 2407001, 2.0 Ci/mmol) was from MP Biomedical. Bafilomycin A1 (cat. # BML-CM110-0100)) was from Enzo Life Sciences. MOG peptide (amino acids 35-55) (cat. # BP001328-PRO-371) was from Syd Labs. OVA peptide (amino acid 323-336) (sequence: ISQAVHAAHAEINE) was synthesized from Tufts University Core facility (Medford, MA, 02155). CFA (cat. # 231131) and heat-inactivated Mycobacterium tuberculosis were from DIFCO Laboratories. Sodium fluoride (NaF, cat # S299-500), sodium chloride (NaCl, cat # S271-10), and Tris (cat BP152-5) were from Fisher Chemicals. Pertussis toxin was from ENZO Life Sciences. ECL development reagent (cat. # 32106), BSA for bicinchoninic acid assay (cat # 23209), and PMSF (cat # 36978) were from Thermo-Scientific. CFSE (cat. # C34554), Cell Trace Violet stain (cat # C34557), RPMI-1640 (cat. # SH30027.02), Penicillin/streptomycin (cat. # 15140-122) and FBS (cat. # 10427-028; lot # 1662765A120-01) were from Life Technologies. Live/dead fixable blue dead cell stain kit was from Molecular Probes. IL-2 ELISA kit (cat. # M2000) was from R&D Systems, Inc.

Antibodies—Anti-CD28 (cat. # 122007) and anti-LFA-1(cat. #141011) were from Biolegend. Anti-CD3Ɛ **(referred to as anti-CD3 in this manuscript)** (cat. # 553064, and 553057), anti-CD25 (cat. # 558642), anti-CD4 (cat. # 553051, and cat # 553047), anti-CD8a (cat. #560469), anti-CD28 (cat. # 553294) and anti-CD44 (cat. # 553135) were from BD Bioscience. Anti-B220 (cat. # 25-0452-81), and anti-CD3Ɛ **(referred to as anti-CD3 in this manuscript)** (cat. # 56-0032-80) were from eBioscience. Anti-HSC70 (cat. #sc-7298) and anti-LAMP1 1D4B (cat. # sc-19992) were from Santa Cruz Biotechnology. Anti-EHD1 (cat. # ab109311) was from Abcam. Anti-ß-Actin (cat. # A5316) was from Sigma-Aldrich. APC-conjugated anti-Annexin V (cat. # 17-8007-72) was from eBiosciences. Polyclonal rabbit antibodies recognizing EHD1 plus EHD4, EHD2 or EHD3 have been described previously (45). Secondary fluorochrome-conjugated antibodies were from Life Technologies.

Mice Generation & Genotyping

Whole-body knockout mice (Ehd1-null) derived from Ehd1flox/flox mice have been described previously (49). Ehd1-null mice were maintained on mixed 129, B6 background. *EHD1$^{fl/fl}$; EHD3$^{fl/fl}$; EHD4$^{fl/fl}$* mice in a predominantly C57BL/6 background were crossed with *B6. Cg-Tg (Cd4-cre) 1Cwi/BfluJ* to generate *Cd4-cre; EHD1$^{fl/fl}$; EHD3$^{fl/fl}$; EHD4$^{fl/fl}$* mice. These mice were further crossed with *C57BL/6-Tg (Tcra2D2, Tcrb2D2)1Kuch/J, 2D2 Tcr or MOG Tcr* to generate *Cd4-cre; 2D2Tcr; EHD1$^{fl/fl}$; EHD3$^{fl/fl}$; EHD4$^{fl/fl}$* mice. *EHD1$^{fl/fl}$; EHD3$^{fl/fl}$; EHD4$^{fl/fl}$* mice in a predominantly C57BL/6 background were also crossed with tamoxifen-inducible CreERT2 expressing mice from Jackson Laboratories (*Gt (ROSA)26Sor$^{tm1(cre/ERT2)\ Tyj}$*; strain 008463) to generate *Cre^{ERT2}; EHD1$^{fl/fl}$; EHD3$^{fl/fl}$;*

EHD4$^{fl/fl}$ mice. These mice were further crossed with *C57BL/6-Tg (Tcra2D2, Tcrb2D2)1Kuch/J, 2D2 Tcr or MOG Tcr)* to generate *Cre^{ERT2}; 2D2Tcr; EHD1$^{fl/fl}$; EHD3$^{fl/fl}$; EHD4$^{fl/fl}$* mice. Genotypes were confirmed by subjecting tail clip DNA to PCR analysis using the KAPA mouse genotyping kit (KAPA Biosystems). Mice were treated humanely according to the National Institutes of Health (NIH) and University of Nebraska Medical Center guidelines. Animal studies were pre-approved by the Institutional Animal Care and Use Committee (#14-067).

Western blotting

Lymphoid tissues or isolated cells were lysed in ice-cold Triton X-100 lysis buffer (0.5% Triton X-100, 50 mM Tris pH 7.5, 150 mM NaCl, 1mM PMSF, 10mM NaF, 1mMVO4) or with RIPA lysis buffer (same as Triton X-100 lysis buffer with an increase of Triton X-100 to 1% and an addition of 5mM EDTA, 1mM EGTA, 1% SDS, and 0.5% sodium deoxycholate). Lysates were vortexed, centrifuged at 13,000 rpm for 30 minutes at 4° C either immediately or after overnight rocking in the cold room and supernatants were collected. Protein lysates were quantified using the bicinchoninic acid (BCA) assay. 40μg aliquots of lysate protein per sample were resolved by SDS/PAGE and transferred to PVDF membranes (from Immobilon-P, cat # IPVH00010). In certain experiments, lysates from equal numbers of cells were resolved by SDS/PAGE. The membranes were blocked in TBS/5% BSA, incubated with the appropriate primary antibodies diluted in TBS-0.1% Tween 20 for 1 hr, washed in TBS-0.1% Tween (3× for 5 minutes each) followed by a 45-min incubation with HRP-conjugated secondary antibody in the same buffer. The membrane was then washed in TBS-0.1% Tween (3× for 5 minutes each) and ECL-based detection was performed.

CD4^{+}T-cell isolation

To isolate primary CD4^{+} T-cells, a negative selection protocol was performed as described (50) using magnetic beads (Invitrogen Biotin binder kit cat. # 11533D) and biotinylated antibodies (Biolegend), and purity was established to be 91–95% based on flow cytometry.

Fluorescence Activated Cell Sorting (FACS)

T-cells were incubated on ice in the dark for 15 to 30 min (depending on the experiment) with appropriate conjugated antibodies at the manufacturer's recommended dilution in FACS buffer (0.1% BSA in PBS). Cells were pelleted, washed twice, and suspended in 400 μl of cold FACS buffer. In other cases, cells were fixed with 4% cold PFA for 15 min at room temperature after staining; then washed and suspended in 400 μl of cold FACS buffer. Cells were protected from light until analyses using either LSR II Green or LSR II cytometer (BD Bioscience). FACS data was analyzed using DIVA (BD FACSDIVA TM Software), FlowJo (FLOWJO, LLC Data Analysis Software, Ashland, OR) and ModFit LT software (Verity Software House, Topsham, ME).

CFSE dye dilution and Cell Trace VioleT-cell proliferation assays

Spleen cells (5×10^{6}cells/ml) from *CD4-Cre; 2D2Tcr; EHD1$^{fl/fl}$; EHD3$^{fl/fl}$; EHD4$^{fl/fl}$* mice and control *(2D2Tcr; EHD1$^{fl/fl}$; EHD3$^{fl/fl}$; EHD4$^{fl/fl}$)* mice were stained with CFSE or

CellTrace Violet according to the manufacturer's instructions. Cells were treated with 50 μg/ml of MOG_{35-55} peptide for 72 hrs. On the indicated day, cells were stained with FITC-CD4 before analysis. Dilution of CFSE or CellTrace Violet fluorescence as an indicator of cell division was assessed via FACS analysis. Data were analyzed using FlowJo and ModFit LT software to delineate percentage of cells that had undergone increasing number of divisions and to determine the Proliferation Index (PI). In some instances, the cells were not stained with the proliferation dye, but were stained with anti-AnnexinV and Propidium Iodide staining solution after 72 hrs of stimulation and analyzed by FACS for cell death analysis.

^{3}H-thymidine incorporation assay and T-cell expansion

Spleen cells (5×10^5 cells/well) from *CD4-Cre; 2D2Tcr; EHD1$^{fl/fl}$; EHD3$^{fl/fl}$; EHD4$^{fl/fl}$* or control *(2D2Tcr; EHD1$^{fl/fl}$; EHD3$^{fl/fl}$; EHD4$^{fl/fl}$)* mice were seeded in 96-well U-bottom plates in 100 μl medium in the presence of varying concentrations of MOG_{35-55} peptide for 72 hrs. Cells were pulsed with1 μCi of ^{3}H-thymidine per well for the last 6 hrs of incubation, harvested onto filter disks and the radioactivity (counts per minute) counted using a scintillation counter (Packard). For T-cell expansion, spleen cells or LN cells from *CD4-Cre*; *2D2Tcr*; *EHD1$^{fl/fl}$*; *EHD3$^{fl/fl}$; EHD4$^{fl/fl}$* mice and control *(2D2Tcr*; *EHD1$^{fl/fl}$*; *EHD3$^{fl/fl}$; EHD4$^{fl/fl}$*) mice were stimulated with 10–20 μg/ml of MOG_{35-55} peptide and T-cells were expanded in the presence of 30 U/ml IL-2 for 7–8 more days (fresh IL-2 containing media every two days after three days of stimulation).

In-vitro deletion of EHD (EHD1, 3 and 4) genes

Spleen cells or LN cells from *EHD1$^{fl/fl}$; EHD3$^{fl/fl}$; EHD4$^{fl/fl}$; Cre^{ERT2}; 2D2Tcr* mice were pre-stimulated with either the MOG peptide or with anti-CD3 and ant-CD28 for three to four days in the presence (+) or absence (−) of 4-hydroxytamoxifen (4-OHT) (200 nM–300 nM) for deletion of EHD 1, 3 and 4. Cells were washed in PBS, stained with CFSE, and were re-stimulated for proliferation as previously described.

ELISA

Isolated spleen cells (5×10^5 cells/well) were cultured in 96-well U-bottom plates in the presence of 10 μg/ml of MOG_{35-55} peptide at 37°C for indicated time points. IL-2 secretion was measured in culture supernatants using an ELISA kit according to the manufacturer's instructions.

Cell surface TCR internalization assay

Internalization of cell surface pool of TCR-CD3 was assessed as previously described (13, 51) with modifications. Briefly, freshly isolated LN cells at 5×10^6 cells/ml in 96-well U-bottom plates (in triplicates) were incubated in the presence of 10 μg/ml BFA at 37°C for the indicated times to allow the surface TCR to internalize in the absence of newly synthesized TCR transport to the cell surface. At each time point, cells were transferred to ice and subsequently stained with PE-conjugated anti-CD3 followed by FACS analysis to quantify the surface TCR levels remaining at each time point. The extent of the TCR remaining at the

cell surface was calculated by expressing the median fluorescent intensity (MFI) of PE-anti-CD3 staining at each time point relative to time 0, which was set as 100%.

Analysis of TCR recycling

The recycling of pre-existing intracellular pools of TCR-CD3 was carried out by adapting a previously described protocol (52). Briefly, the accessibility of the cell surface CD3 on freshly isolated LN cells (at 5×10^6 cells/ml in 96-well U-bottom plates in triplicates) was blocked by staining with a predetermined saturating concentration of unconjugated anti-CD3 at 4°C for 30 min. The cells were extensively washed and incubated at 37°C. At the indicated times, the cells were transferred to 4°C and stained with a PE-conjugated version of the same anti-CD3 antibody that was used to block the staining of the initial cell surface cohort of CD3. The MFI of PE-anti-CD3 cell surface FACS staining was used as a measure of the recycling of intracellular TCR-CD3. Recycling of cell surface TCR-CD3 pool following internalization was assayed by a modified protocol (53, 54). Freshly isolated LN cells were first stained with PE-conjugated anti-CD3 for 30 min on ice. After extensive washes, the cells were incubated at 37°C for 30 min (in complete RPMI) to allow the antibody-labelled TCR-CD3 to undergo internalization. The cells were then subjected to an acid wash to strip any remaining antibody bound to CD3 on T-cell surface. The cells were washed in cold FACS buffer and re-suspended in complete RPMI followed by incubation at 37°C for the indicated times to allow recycling of the labelled internalized pool of TCR-CD3 back to the cell surface. The cells were spun down, acid washed, and re-suspended in FACS buffer for FACS analysis to determine the remaining intracellular fraction of the internalized TCR-CD3. The percentage of TCR-CD3 recycling was calculated from the equation $((T_0-T_x)/T_0) \times 100$, where T_0 is the MFI of cells incubated for 0 min before he second acid wash, while T_x is the MFI of cells subjected to a second acid wash after incubation for the indicated times.

Confocal Microscopy

Lymph node T-cells were expanded as described under T-cell expansion. A total of 5×10^6 expanded T-cells in complete RPMI medium were plated onto Poly-L-lysine-coated coverslip placed in 24-well plates and allowed to attach at 37°C for 10 min. Cells on coverslips were fixed in 4% ice-cold PFA for 20 min and then incubated with 0.1M glycine (in PBB) for 3 min at room temperature. After washing, the cells were incubated with the blocking plus permeabilization buffer (2% BSA +0.1% Triton in PBS) for 30 min at room temperature. Cells were stained with anti-Lamp-1 and anti-CD3 primary antibodies overnight a 4°C. After three washes, the cells were stained with secondary anti-rat (for Lamp-1) and anti-Armenian hamster antibodies for 45 min at room temperature. After washes, the cells were mounted with VECTASHIELD Hard Set mounting medium with DAPI (Vector laboratories, Cat # H-1500). Images were acquired at room temperature using ZEISS ELYRA S.1 or a Super-Resolution Structured Illumination (SR-SIM) microscopy. The sCMOS camera mounted on side port was used. Objective lenses: Plan-APOCHROMAT 63×/1.40 Oil DIC. For resolution: lateral resolution (XY): 120 nm, axial resolution (Z): 300 nm (typical experimental FWHM values with objective lens Plan-APOCHROMAT 63×/1.40 Oil DIC, sub-resolution beads of 40 nm diameter and excitation

at 488 nm). Merged fluorescence pictures were generated and analyzed using ZEN ®2012 software from Carl Zeiss.

Induction and monitoring of Experimental Autoimmune Encephalomyelitis (EAE)

Six to eight week old female *CD4-Cre*; *2D2Tcr*; *EHD1*$^{fl/fl}$; *EHD3*$^{fl/fl}$*; EHD4*$^{fl/fl}$ or control *(2D2Tcr*; *EHD1*$^{fl/fl}$; *EHD3*$^{fl/fl}$*; EHD4*$^{fl/fl}$) mice were subcutaneously immunized in the flank with 200 μg of MOG_{35-55} peptide emulsified (1:1) in complete Freund's adjuvant (CFA) containing 0.5 mg heat-killed *Mycobacterium tuberculosis* H37RA in a total of 200 μl emulsion per mouse, together with an intraperitoneal injection of pertussis toxin (200 ng/mouse) in 200 μl PBS followed by a second dose of pertussis toxin two days later. Mice were monitored daily and scored for clinical signs of EAE on a scale of 0–5 whereby 0 = no disease; 1 = decrease tail tone; 2 = hind limb weakness or partial paralysis; 3 = complete hind limb paralysis; 4 = front and hind limb paralysis; and 5 = moribund state or dead (55). Composite scores of each cohort were used to determine statistical significance.

Statistics

An unpaired student's *t* test was used to calculate the *p*-values. Data is presented as mean ± SEM and $p<0.05$ served as the threshold for statistical significance.

RESULTS

Multiple EHD family members are expressed in lymphoid organs and purified CD4$^+$ T-cells

Our previous Western blotting studies of EHD protein expression in the mouse thymus and spleen (49, 56, 57), which we extended here to lymph nodes (LN) (Fig. 1A), showed that multiple EHD family members are expressed, albeit unequally, in lymphoid organs. This suggested that multiple EHD family members are likely to be expressed in individual immune cell types, consistent with our recent findings that bone marrow derived macrophages (BMDMs) express both EHD1 and EHD4 (36). With the focus of this study on functional analyses in the context of CD4$^+$ T-cells, our additional analyses showed that EHD 1, 3 and 4 are expressed in primary murine CD4$^+$ T-cells (Fig. 1B) while EHD2 protein was undetectable to barely detectable (Fig. 1C). Analyses of mRNA expression databases (ImmGen and BioGPS) further support this expression pattern (S Fig. 1). Notably, western blotting of purified LN T-cells at various time points of anti-CD3/CD28 stimulation showed that levels of EHD proteins vary as a function of CD4$^+$ T-cell activation, with a time-dependent increase in EHD 1 and 4 levels and a reduction in EHD3 levels (Fig. 1B). These findings suggested that EHD proteins may play important roles in T-cell function.

Our previous knockout studies have revealed relatively unique as well as redundant functional roles of EHD proteins, with the knockout of EHD1 alone producing by far the most obvious developmental and adult organ functional aberrations, depending on the strain background (27, 37, 38, 49). Therefore, we assessed whether EHD1 deficiency had any impact on T-cell activation. Notably, the initial analysis of EHD1$^{-/-}$ splenic T-cells did not reveal any detectable abnormality in anti-CD3/CD28 induced cell proliferation (Fig. 2A). These findings supported a redundant functional role of EHD proteins, at least in the context of T-cell proliferation. Consistent with this, a slight increase in EHD4 levels was noted in

LN from EHD1$^{-/-}$ mice (Fig. 2A). Initial analysis of EHD3$^{-/-}$ CD4^{+} T-cells showed no difference in anti-CD3/CD28 induced proliferation compared to CD4^{+} T-cells from control mice (Fig 2B). We observed that deletion of EHD3 did not cause an increase in the level of either EHD1 or EHD4 in lymph node cells (Fig. 2B). However, EHD4$^{-/-}$ CD4^{+} T-cells showed reduced proliferation compared to control CD4^{+} T-cells although the decrease was not statistically significant (Fig. 2C). We also noted that the deletion of EHD4 did not cause an increase in the level of either EHD1 or EHD3 in lymph node cells. Given the lack of impact or a mild impact of single EHD gene knockouts on T-cell proliferation and the expression of multiple family members, we reasoned that EHD1, 3 and 4 might function redundantly in T cells, we used a combinatorial knockout strategy to further explore their role in T-cells.

CD4-Cre mediated conditional deletion of EHD1/3/4 in T-cells leads to a reduced proportion of CD4^{+} T-cells in secondary lymphoid tissues

Given the likelihood of redundant EHD function, we generated mice with a CD4-Cre-depepndent, T-cell directed, conditional deletion of floxed *Ehd1*, *Ehd3*, and *Ehd4* genes. To examine the impact of EHD 1/3/4 deletions in T-cells in the context of antigen-specific responses, we also incorporated the MOG peptide-specific *2D2-Tcr* transgene (55) into our conditional knockout model (referred to as CD4-Cre^{+} mice). Littermates without a *CD4-Cre* transgene were used as controls (referred to as CD4-Cre^{-} mice). The presence of floxed EHD1/3/4 gene alleles targeted for CD4-Cre-dependent deletion was detected by tail PCR using specific primers for each floxed allele (S Fig. 2A). Western blot analysis of CD4^{+} T-cells isolated from the *2D2-Tcr* transgenic mice showed that the presence of the transgenic TCR by itself did not have any significant impact on the levels of EHD proteins (S Fig. 2B). CD4-Cre^{+} mice were developmentally indistinguishable from CD4-Cre^{-} mice and no gross phenotypic changes were seen in adult mice. Western blot analysis confirmed the CD4-dependent deletion of EHD1/3/4 (Fig. 3A).

Next, to examine whether EHD1/3/4 deletion impacted T-cell development, we isolated single cells from lymphoid organs of 4-week-old mice and analyzed these for changes in T-cell numbers using cell counting combined with FACS. We found that total numbers of thymocytes, splenocytes, and LN cells were comparable in mice from both groups (Fig. 3B). Similarly, comparable cell numbers were observed when spleens of older (6–8 weeks old) mice of the two genotypes were analyzed (Fig. 3C). We carried out FACS analyses on the live/B220^{-} T-cell population, and assessed the proportion of cells at various developmental stages based on staining with antibodies against CD4, CD8, CD25 and CD44 (58–60). Single positive thymocytes in *2D2-Tcr* Tg mice are known to be skewed toward the CD4^{+} T-cell compartment; this is also seen in spleen and LN (55). CD4-Cre mediated deletion of EHD 1/3/4 did not affect the relative percentages or total cell numbers within various thymic developmental stages when analyzed in 4-week-old mice (Fig. 3D and 3E).

In contrast, CD4-Cre mediated EHD1/3/4 deletion led to a decrease in the percentage of T-cells in the periphery. This phenotype was seen in both the LN and spleen (Fig. 3F, 3G), although only the splenocyte reduction was statistically significant. However, the absolute number of CD4^{+} T-cells in these organs did not differ significantly between the CD4-Cre

positive and control mice. In addition, an apparent increase in peripheral B cell numbers and their percentages were seen (Fig. 3F, 3G); the basis of this phenotype is unknown but is likely to reflect altered T-cell/B-cell interactions due to T-cell deficiency of EHD1/3/4. We also saw a decrease in the percentage of $CD8^+$ T-cells in spleens of CD4-Cre positive mice, but this did not reflect an increase in $CD8^+$ T-cell numbers in these organs. From these results, we conclude that expression of EHD proteins is dispensable during thymic T-cell development, but may play a role in peripheral T-cell function. To exclude the possibility that the lack of impact on T-cell development and changes in peripheral lymphocyte numbers might reflect the presence of an autoreactive TCR transgene, we also analyzed the non-TCR-transgenic mice for the effect of CD4-Cre-mediated EHD1/3/4 deficiency during thymic development and in spleen cells. We observed a lack of impact of T-cell development like that seen in the TCR transgenic mice (Fig. 4A, 4B, 4C), further supporting the conclusion that EHD proteins are dispensable for thymic T-cell development beyond the $CD4/8^+$ stage. The analysis of spleen cells showed a slight increase in the percentage of $B220^+$cells (B-cells) and a slight decrease in the percentages of $CD4^+$ and $CD8^+$ T-cells, but these differences were not statistically significant (Fig. 4D).

Expression of EHD proteins is required for optimal antigen-induced T-cell activation in vitro and for EAE in vivo

Incorporation of a MOG antigen-specific TC transgene in our EHD1/3/4 deletion models allowed analyses of $CD4^+$ T-cell response to a specific antigen, both in vitro and in vivo, the latter in the context of the development of EAE. We asked whether the mature T-cells in these mice exhibit any functional deficits. Initial experiments using spleen cells from the parental 2D2-TCR transgenic and control mice with MOG or ovalbumin peptides, established the optimal concentrations of MOG peptide to induce T-cell proliferation (not shown). Analysis of $CD4^+$ T-cells from spleen using the CellTrace Violet stain and ^{3}H-thymidine incorporation showed a significant decrease proliferation of T-cells from CD4-Cre^+ mice compared to control CD4-Cre^- (Fig. 5A, 5B). Visualization of progressive cell divisions using ModFit LT software, showed that while CD4-Cre^+ and CD4-Cre^- $CD4^+$ T-cells progress through a comparable number of divisions, EHD1/3/4-null T-cells exhibit a significant underrepresentation at late divisions and an increased proportion of cells at earlier divisions (Fig. 5A). The EHD1/3/4-null T-cells also exhibited a significantly lower overall proliferation index (Fig. 5A), further supporting the conclusion that these cells proliferate slower than the control T-cells. To exclude the possibility that the apparent decrease in the number of EHD1/3/4-null T-cells at late stages of proliferation might be due to their apoptosis, we stimulated the $CD4^+$ T-cells as previously described and stained these with PI and anti-Annexin V followed by FACS analysis. We observed no increase in the percentage of apoptotic cells in antigen-stimulated $CD4^+$ T-cells isolated from CD4-Cre^+ compared to CD4-Cre^- (control) mice (Fig. 5C). Thus, the mature peripheral $CD4^+$ T-cells of CD4-Cre^- exhibit a marked defect in the specific antigen-induced cell proliferation in vitro.

To assess whether the impact of EHD1/3/4 protein deficiency on $CD4^+$ T-cell proliferation reflects their abnormal development or an actual importance in the events associated with T-cell activation, we used T-cells from *2D2-TCR Tg*-bearing mice carrying a tamoxifen-

inducible ERT-Cre that allows *in vitro* deletion of EHD1/3/4. EHD1/3/4 deletions in vitro led to a significant decrease in antigen-induced proliferation compared to their control T-cells (Fig. 5D, 5E, 5F). These results support a T-cell intrinsic positive role of EHD proteins in sustaining antigen-driven T-cell responses in mature peripheral T-cells.

Among the cytokines that initiate antigen-activated T-cells into proliferation is the activation-induced secretion of IL-2 and the induced expression of the corresponding receptor on the T-cell surface (61, 62). Therefore, we assessed the impact of EHD1/3/4 deletions on IL-2 secretion. We observed a significantly lower level of antigen-induced IL-2 secretion by EHD1/3/4-null $CD4^+$ T-cells (Fig. 5G) with a difference detectable at the earliest time point (12 hrs.) analyzed, making it unlikely that the reduction is due to a smaller pool of T-cells caused by reduced proliferation. The significant reduction in IL-2 secretion is likely to represent one mechanism for the defective T-cell proliferation upon deletion of EHD1/3/4.

The impact of EHD1/3/4 deficiencies was not restricted to in vitro T-cell responses alone. Using immunization with the MOG_{35-55}, we could test the impact of EHD1/3/4 deficiencies on the development of EAE *in vivo*. We immunized cohorts of control ($CD4\text{-}Cre^-$) vs. experimental ($CD4\text{-}Cre^+$) mice with MOG_{35-55} and assessed onset and severity of EAE over time. Interestingly, while no significant difference in the disease onset was seen, EHD1/3/4 –null group showed a decrease in the disease severity compared to control littermates (Fig. 5H). These results further support our conclusion that the expression of EHD proteins is important for full $CD4^+$ T-cell responses to antigen. Altogether, these *in vitro* and *in vivo* analyses established, for the first time, that EHD proteins play an important positive role in antigen-driven T-cell activation and immune response.

EHD proteins regulate the traffic of the TCR-CD3 complex to the cell surface

At a cellular level, EHD proteins have been characterized as regulators of the endocytic traffic of different cell surface receptors as mentioned in the introduction. Endocytic traffic of these receptors is also key to their targeting to the immunological synapse (1, 10–13, 63–66). To assess whether EHD proteins may indeed regulate the traffic of TCR-CD3 or the accessory receptors, we first examined the cell surface levels of TCR-CD3, CD28, CD4, CD25, CTLA-4 and LFA-1 by FACS analysis of unstimulated T cells (Fig. 6A). As assessed by comparing the MFI values, T-cells from $CD4\text{-}Cre^+$ mice expressed significantly lower levels of TCR-CD3 on the cell surface compared to T-cells from control mice (Fig 6A, 6C). These analyses also showed that in vitro activated $CD4^+$ T-cells from $CD4\text{-}Cre^+$ mice express lower levels, although not statistically significant, of TCR-CD3, CD28, CD4, CD25, CTLA-4 and LFA-1 compared to those from control mice (Fig. 6B, 6C).

Since the TCR-CD3 complex is the primary determinant of antigen-specific T-cell activation and subsequent responses, we focused on the TCR for further analyses. We examined the kinetics of TCR-CD3 internalization and recycling in unstimulated $CD4^+$ T-cells. Analysis of TCR-CD3 internalization using FACS showed that there was not significant difference in internalization of TCR in EHD1/3/4 -null T-cells compared to control T-cells (Fig. 7A). Next, we analyzed recycling to the cell surface of the pre-existing intracellular pool of TCR/CD3. For this purpose, anti-CD3ε antibody recognition epitope on the pre-existing surface

TCR-CD3 was blocked with an un-conjugated antibody and the appearance of intracellular TCR-CD3 on the cell surface at various time points was monitored by staining with a conjugated anti-CD3Ɛ. These analyses revealed that EHD1/3/4 -null $CD4^+$ T-cells exhibit a significantly reduced recycling of pre-existing intracellular TCR-CD3 to the cell surface at all-time points analyzed compared to control T-cells (Fig. 7B). Next, we assessed the recycling of the pre-existing cell surface pool of TCR-CD3 by pre-labelling it with a PE-conjugated anti-CD3 and allowing it to internalize. After acid wash (to strip any remaining antibody bound to TCR-CD3 on T-cell surface), the internalized PE-labeled TCR-CD3 was allowed to reappear at the cell surface and re-stripped to remove the labeled antibody. Even under these assay conditions, we observed a significant decrease in the recycling of TCR-CD3 in EHD1/3/4 -null $CD4^+$ T-cells compared to control cells (Fig. 7C). Overall, these results show a key requirement of EHD 1, 3 and 4 in basal recycling of TCR-CD3 from intracellular endocytic recycling compartments back to the cell surface.

Deletion of EHD1, 3 and 4 promotes the lysosomal degradation of TCR-CD3

Given the impairment of the endocytic recycling (Fig. 7B, 7C) together with the reduced steady-state surface TCR-CD3 levels in freshly-isolated EHD1/3/4-null T cells (Fig. 6), we considered the possibility that the pool of TCR-CD3 that is retained in intracellular compartments may be aberrantly targeted for lysosomal degradation. To address this, EHD1/3/4-null T cells (from CD4-Cre-mediated and 4OHT-induced ERT-Cre deletion) were examined by WB for total levels of CD3Ɛ. In both cases, we found that deletion of EHD proteins led to a significant decrease in the total levels of CD3Ɛ (Fig. 8). As in unstimulated T cells, we also observed a reduction in the total level of CD3Ɛ in activated $CD4^+$ T-cells (Fig. 8C). Given our findings with the CSF-1 receptor in macrophages (36), we hypothesized that this reduction was likely due to lysosomal targeting and degradation. To test this hypothesis, we treated the EHD1/3/4-null T-cells with or without Bafilomycin-A1, an inhibitor of lysosomal degradation, for 4 h and analyzed the impact on total CD3Ɛ levels using WB and confocal (Fig. 9). WB of cells treated with Bafilomycin-A1 for 4 h showed a recovery of the CD3Ɛ protein level in EHD1/3/4 -null T-cells with levels comparable to those in control cells (in treated cells) (Fig. 9A, 9B). We performed confocal imaging of control and EHD1/3/4 -null T cells incubated with or without Bafilomycin-A1. While relatively low CD3Ɛ staining was co-localized with the lysosomal marker LAMP-1 in untreated cells (Fig. 9D), some co-localization was seen in Bafilomycin A1-treated control T cells (Fig. 9C, upper). Notably, significantly more lysosome-localized CD3Ɛ was seen in EHD1/3/4 -null cells treated with bafilomycin-A1 (Fig. 9C, lower, and Fig. 9E). These results support the conclusion that expression of EHD1/3/4 is required for efficient transport of TCR-CD3 from endosomal compartments back to the cell surface and to prevent its aberrant traffic into lysosomes.

DISCUSSION

Cellular studies have identified members of the EHD protein family as key new regulatory elements of endocytic trafficking of several cell surface receptors, but their physiological functions remain relatively unexplored and their roles in the immune system unknown. Here, we investigate the role of EHD proteins in the context of antigen-specific $CD4^+$ T-cells *in*

vitro and *in vivo*. Our genetic studies, ablating genes encoding three members of the EHD protein family (EHD 1, 3 and 4) by $CD4^+$ T-cells in the context of MOG transgenic TCR, demonstrate for the first time, an important, positive role of EHD proteins in antigen-specific T-cell activation *in vitro* and an autoimmune response *in vivo*. Mechanistically, we show that EHD proteins are required for basal recycling of TCR-CD3 from intracellular endocytic pools to the cell surface, thereby determining the subsequent level of T-cell activation. Combined with our recent study demonstrating a key positive role of EHD1 in the transport of newly synthesized CSF-1R from the Golgi to the cell surface of BMDMs (36), and previous cell biological findings that EHD1 facilitates MHC class I recycling from the endocytic recycling compartment to the cell surface in a cell line system (25), our results strongly support the likelihood that EHD proteins play critical and potentially diverse roles in the immune system.

Analysis of thymic T-cell development did not reveal any significant alterations in total cellularity, T-cell subsets or relative proportions of T-cells at various developmental stages in mice with a CD4-Cre mediated deletion of EHD1/3/4, indicating that EHD proteins are largely dispensable for thymic development beyond the CD4/8 double-positive stage. Whether this might reflect any role of the remaining EHD family member, EHD2, remains a possibility that will require future studies. It is also possible that EHD proteins are important at earlier stages of thymic development and future use of other Cre elements active at these stages will be needed to address this possibility.

In contrast to the relatively unperturbed thymic development, CD4-Cre mediated EHD1/3/4 deletion led to a decrease in the percentage of T-cells in the periphery. This phenotype was seen in secondary lymphoid tissues, including the lymph nodes and the spleen, but was only significant in the spleen. These results suggested that EHD proteins may play a more important role in mature peripheral T-cells. The precise basis for this phenotype remains unclear but lower functional responses to TCR engagement, as seen in *ex vivo* analyses (discussed below), could play a role since TCR signals are important in peripheral T-cell maintenance (67–69). In addition, an apparent increase in the peripheral B cell numbers and their percentages were seen in the EHD1/3/4-null mice in the context of 2D2 transgene; the basis of this phenotype is unknown but is likely to reflect altered T-cell/B-cell interactions due to T-cell deficiency of EHD1/3/4 genes. There was also a decrease in the percentage of $CD8^+$ T-cells in the periphery, but this was only significant in the spleens of transgenic mice. Further studies will be needed to precisely assess the basis of these effects.

The in *vitro* analyses of T-cells from the CD4-Cre deletion model demonstrated significantly defective antigen-elicited $CD4^+$ T-cell proliferation and IL-2 cytokine secretion responses upon EHD1/3/4 deletion. Similar results were observed using $CD4^+$ T-cells derived from an alternate model where in vitro deletion of floxed EHD1, 3 and 4 genes was induced with 4-OHT to bypass any *in vivo* developmental abnormalities. These results support a T-cell intrinsic positive role of EHD proteins in sustaining antigen-driven T-cell responses in mature peripheral T-cells, a role independent of any potential involvement of EHD proteins in events associated with thymic T-cell development.

Coordination of multiple EAE-inducing T-cell functions, including their early activation, expansion, migration to the brain across the blood/brain barrier, and effector functions to mediate demyelination in the CNS are required for full disease induction (70, 71). Therefore, we analyzed the impact of EHD1/3/4 deficiencies on the onset and progression of EAE. Since *in vitro* studies showed the T-cell proliferation and cytokine (IL-2) secretion to be impaired upon EHD1/3/4 deficiencies, we expected to see a delayed onset and reduced severity of EAE. While we saw no difference in the onset of disease, EHD1/3/4-null mice showed a decrease in the disease severity compared to control littermates. Therefore, further *in vitro* and *in vivo* studies using models developed here should help to comprehensively reveal other aspects of T-cell function that also rely on EHD protein expression.

Given the reduced TCR-CD3 levels in the $CD4^+$ T-cells of our EHD1/3/4 -null mouse model prior to deliberate T-cell activation, our focus here has been on the role of EHD proteins in basal (prior to antigenic stimulation) TCR-CD3 traffic, which has not been mechanistically dissected in much detail. Therefore, further studies to identify partner proteins through which EHDs regulate TCR traffic will be of great interest. Notably, endocytic trafficking pathways play key roles during T-cell activation by orchestrating the polarized transport of TCR-CD3 and signaling molecules such as Lck to maintain an active immunologic synapse, and Rab4- and $Rab11^+$ endosomes are implicated in these processes (72).

Cell biological studies have linked EHD proteins to the regulation of traffic in $Rab11^+$ recycling endosomes as well as compartments regulated by other Rabs. Thus, further studies to examine the potential importance of EHD proteins in regulating endocytic traffic into and out of the IS during T-cell activation will be of great interest. In this regard, we and others have recently identified a key role of EHD proteins in primary cilia biogenesis (37, 42) and recent studies have shown that the maintenance of IS in cilia-less T-cells involves ciliogenesis-related proteins such as IFT20 which localize in the IS and are required for recycling of TCR-CD3 (46, 47, 73). Although IFT20 KO under CD4-Cre led to only minor defects in T-cell development and collagen-induced arthritis (an experimental model of rheumatoid arthritis), earlier deletion using Lck-Cre led to defective thymic development and T-cells function *in vivo* (74); the latter are partially similar to the phenotype of our EHD1/3/4 KO mice. Interestingly, the requirement of EHD1 and EHD3 were found to be important for the recruitment of transition zone proteins and IFT20 during ciliary vesicle formation (42). Though our study has been done mainly on freshly isolated and rested cells, it seems plausible that EHD proteins may also regulate the traffic of TCR-CD3 in the IS to promote T-cell activation and subsequent responses.

Notably, the CD4-Cre mediated Wiskott-Aldrich syndrome protein and SCAR homolog (WASH) deletion led to T-cell defects strongly resembling the phenotype of EHD1/3/4 deficiency with minimal thymic developmental defects, reduced proliferation and cytokine production, a decrease in the surface TCR-CD3 levels, increase in lysosomal degradation of TCR-CD3, and reduced severity of EAE (75). WASH is an Arp2/3 activator that localizes on distinct endosomal subdomains and functions in endosomal trafficking (76). Given these phenotypic similarities of the two KO models and the interaction of the WASH protein with retromer complex and the involvement of EHD proteins in retromer-dependent transport (77,

78), further exploration of a link between EHD proteins and WASH complex in regulating TCR-CD3 traffic will be of great interest.

Overall, studies presented here using genetic models and functional analyses *in vivo* and *in vitro*, reveal an important albeit redundant positive role of the newly-described EHD family of endocytic recycling regulatory proteins in T-cell function. Mechanistically, we show that EHD proteins are required to facilitate basal recycling of TCR-CD3 from intracellular endocytic compartments back to the cell surface to ensure the surface expression of optimal TCR-CD3 levels for subsequent antigen-driven T-cell activation. Future studies using the unique models described here should add to our understanding of the importance of endocytic traffic in the control of TCR-CD3 and other receptors that regulate T-cell functions as well as the roles of these proteins in other cells in the innate and adaptive arms of the immune system.

Supplementary Material

Refer to Web version on PubMed Central for supplementary material.

Acknowledgments

We thank the members of the Band Laboratories for helpful discussions and Dr. Vijay Kuchroo (Brigham and Women's Hospital, Harvard Medical School) for advice on the use of 2D2 mice.

GRANT SUPPORT

This work was supported by: the NIH grants CA105489, CA87986, CA99163 and CA116552 to HB, CA105489-supplement to FI, and CA96844 and CA144027 to VB; Department of Defense grants W81XWH-07-1-0351 and W81XWH-11-1-0171 (VB); a University of Nebraska System Science Collaborative grant (HB); Institutional Development Award (IDeA) from the NIGMS of the NIH under grant number P30 GM1063. Support for the UNMC Confocal, Flow Cytometry and other core facilities from the NCI Cancer Center Support Grant (P30CA036727) to Fred & Pamela Buffett Cancer Center, NIGMS P30 GM1063, and the Nebraska Research Initiative.

ABBREVIATION USED

EHD	EPS-15 homology domain-containing protein
EAE	Experimental Autoimmune Encephalomyelitis
MOG	Myelin oligodendrocyte Glycoprotein
DN	double negative
DP	double positive
SP	single positive
LN	lymph nodes
WT	wild-type
4-OHT	4-hydroxytamoxifen

References

1. Huppa JB, Gleimer M, Sumen C, Davis MM. Continuous T cell receptor signaling required for synapse maintenance and full effector potential. Nat Immunol. 2003; 4:749–755. [PubMed: 12858171]
2. Hashimoto-Tane A, Yokosuka T, Ishihara C, Sakuma M, Kobayashi W, Saito T. T-cell receptor microclusters critical for T-cell activation are formed independently of lipid raft clustering. Mol Cell Biol. 2010; 30:3421–3429. [PubMed: 20498282]
3. Jo JH, Kwon MS, Choi HO, Oh HM, Kim HJ, Jun CD. Recycling and LFA-1-dependent trafficking of ICAM-1 to the immunological synapse. J Cell Biochem. 2010; 111:1125–1137. [PubMed: 20681010]
4. Lee KH, Dinner AR, Tu C, Campi G, Raychaudhuri S, Varma R, Sims TN, Burack WR, Wu H, Wang J, Kanagawa O, Markiewicz M, Allen PM, Dustin ML, Chakraborty AK, Shaw AS. The immunological synapse balances T cell receptor signaling and degradation. Science. 2003; 302:1218–1222. [PubMed: 14512504]
5. Das V, Nal B, Dujeancourt A, Thoulouze MI, Galli T, Roux P, Dautry-Varsat A, Alcover A. Activation-induced polarized recycling targets T cell antigen receptors to the immunological synapse; involvement of SNARE complexes. Immunity. 2004; 20:577–588. [PubMed: 15142526]
6. Valitutti S, Muller S, Salio M, Lanzavecchia A. Degradation of T cell receptor (TCR)-CD3-zeta complexes after antigenic stimulation. J Exp Med. 1997; 185:1859–1864. [PubMed: 9151711]
7. Naslavsky N, Caplan S. EHD proteins: key conductors of endocytic transport. Trends Cell Biol. 2011; 21:122–131. [PubMed: 21067929]
8. Gould GW, Lippincott-Schwartz J. New roles for endosomes: from vesicular carriers to multi-purpose platforms. Nat Rev Mol Cell Biol. 2009; 10:287–292. [PubMed: 19277045]
9. Walseng E, Bakke O, Roche PA. Major histocompatibility complex class II-peptide complexes internalize using a clathrin- and dynamin-independent endocytosis pathway. J Biol Chem. 2008; 283:14717–14727. [PubMed: 18378669]
10. Cefai D, Schneider H, Matangkasombut O, Kang H, Brody J, Rudd CE. CD28 receptor endocytosis is targeted by mutations that disrupt phosphatidylinositol 3-kinase binding and costimulation. J Immunol. 1998; 160:2223–2230. [PubMed: 9498761]
11. Stanley P, Tooze S, Hogg N. A role for Rap2 in recycling the extended conformation of LFA-1 during T cell migration. Biol Open. 2012; 1:1161–1168. [PubMed: 23213397]
12. Fabbri M, Di Meglio S, Gagliani MC, Consonni E, Molteni R, Bender JR, Tacchetti C, Pardi R. Dynamic partitioning into lipid rafts controls the endo-exocytic cycle of the alphaL/beta2 integrin, LFA-1, during leukocyte chemotaxis. Mol Biol Cell. 2005; 16:5793–5803. [PubMed: 16207819]
13. Liu H, Rhodes M, Wiest DL, Vignali DA. On the dynamics of TCR:CD3 complex cell surface expression and downmodulation. Immunity. 2000; 13:665–675. [PubMed: 11114379]
14. Kumar A, Kremer KN, Dominguez D, Tadi M, Hedin KE. Galpha13 and Rho mediate endosomal trafficking of CXCR4 into Rab11+ vesicles upon stromal cell-derived factor-1 stimulation. J Immunol. 2011; 186:951–958. [PubMed: 21148034]
15. Mintz L, Galperin E, Pasmanik-Chor M, Tulzinsky S, Bromberg Y, Kozak CA, Joyner A, Fein A, Horowitz M. EHD1–an EH-domain-containing protein with a specific expression pattern. Genomics. 1999; 59:66–76. [PubMed: 10395801]
16. Pohl U, Smith JS, Tachibana I, Ueki K, Lee HK, Ramaswamy S, Wu Q, Mohrenweiser HW, Jenkins RB, Louis DN. EHD2, EHD3, and EHD4 encode novel members of a highly conserved family of EH domain-containing proteins. Genomics. 2000; 63:255–262. [PubMed: 10673336]
17. Daumke O, Lundmark R, Vallis Y, Martens S, Butler PJ, McMahon HT. Architectural and mechanistic insights into an EHD ATPase involved in membrane remodelling. Nature. 2007; 449:923–927. [PubMed: 17914359]
18. Blume JJ, Halbach A, Behrendt D, Paulsson M, Plomann M. EHD proteins are associated with tubular and vesicular compartments and interact with specific phospholipids. Exp Cell Res. 2007; 313:219–231. [PubMed: 17097635]

19. Jakobsson J, Ackermann F, Andersson F, Larhammar D, Low P, Brodin L. Regulation of synaptic vesicle budding and dynamin function by an EHD ATPase. J Neurosci. 2011; 31:13972–13980. [PubMed: 21957258]
20. Ioannou MS, Marat AL. The role of EHD proteins at the neuronal synapse. Sci Signal. 2012; 5:jc1. [PubMed: 22534130]
21. Shah C, Hegde BG, Moren B, Behrmann E, Mielke T, Moenke G, Spahn CM, Lundmark R, Daumke O, Langen R. Structural insights into membrane interaction and caveolar targeting of dynamin-like EHD2. Structure. 2014; 22:409–420. [PubMed: 24508342]
22. Lin SX, Grant B, Hirsh D, Maxfield FR. Rme-1 regulates the distribution and function of the endocytic recycling compartment in mammalian cells. Nat Cell Biol. 2001; 3:567–572. [PubMed: 11389441]
23. Grant B, Zhang Y, Paupard MC, Lin SX, Hall DH, Hirsh D. Evidence that RME-1, a conserved C. elegans EH-domain protein, functions in endocytic recycling. Nat Cell Biol. 2001; 3:573–579. [PubMed: 11389442]
24. George M, Ying G, Rainey MA, Solomon A, Parikh PT, Gao Q, Band V, Band H. Shared as well as distinct roles of EHD proteins revealed by biochemical and functional comparisons in mammalian cells and C. elegans. BMC Cell Biol. 2007; 8:3. [PubMed: 17233914]
25. Caplan S, Naslavsky N, Hartnell LM, Lodge R, Polishchuk RS, Donaldson JG, Bonifacino JS. A tubular EHD1-containing compartment involved in the recycling of major histocompatibility complex class I molecules to the plasma membrane. Embo J. 2002; 21:2557–2567. [PubMed: 12032069]
26. Guilherme A, Soriano NA, Furcinitti PS, Czech MP. Role of EHD1 and EHBP1 in perinuclear sorting and insulin-regulated GLUT4 recycling in 3T3-L1 adipocytes. J Biol Chem. 2004; 279:40062–40075. [PubMed: 15247266]
27. Rapaport D, Auerbach W, Naslavsky N, Pasmanik-Chor M, Galperin E, Fein A, Caplan S, Joyner AL, Horowitz M. Recycling to the plasma membrane is delayed in EHD1 knockout mice. Traffic. 2006; 7:52–60. [PubMed: 16445686]
28. Jovic M, Naslavsky N, Rapaport D, Horowitz M, Caplan S. EHD1 regulates beta1 integrin endosomal transport: effects on focal adhesions, cell spreading and migration. J Cell Sci. 2007; 120:802–814. [PubMed: 17284518]
29. Lasiecka ZM, Yap CC, Caplan S, Winckler B. Neuronal early endosomes require EHD1 for L1/NgCAM trafficking. J Neurosci. 2010; 30:16485–16497. [PubMed: 21147988]
30. Curran J, Makara MA, Little SC, Musa H, Liu B, Wu X, Polina I, Alecusan JS, Wright P, Li J, Billman GE, Boyden PA, Gyorke S, Band H, Hund TJ, Mohler PJ. EHD3-dependent endosome pathway regulates cardiac membrane excitability and physiology. Circ Res. 2014; 115:68–78. [PubMed: 24759929]
31. Gudmundsson H, Hund TJ, Wright PJ, Kline CF, Snyder JS, Qian L, Koval OM, Cunha SR, George M, Rainey MA, Kashef FE, Dun W, Boyden PA, Anderson ME, Band H, Mohler PJ. EH domain proteins regulate cardiac membrane protein targeting. Circ Res. 2010; 107:84–95. [PubMed: 20489164]
32. Posey AD Jr, Swanson KE, Alvarez MG, Krishnan S, Earley JU, Band H, Pytel P, McNally EM, Demonbreun AR. EHD1 mediates vesicle trafficking required for normal muscle growth and transverse tubule development. Dev Biol. 2014; 387:179–190. [PubMed: 24440153]
33. Demonbreun AR, Swanson KE, Rossi AE, Deveaux HK, Earley JU, Allen MV, Arya P, Bhattacharyya S, Band H, Pytel P, McNally EM. Eps 15 Homology Domain (EHD)-1 Remodels Transverse Tubules in Skeletal Muscle. PLoS One. 2015; 10:e0136679. [PubMed: 26325203]
34. Posey AD Jr, Pytel P, Gardikiotes K, Demonbreun AR, Rainey M, George M, Band H, McNally EM. Endocytic recycling proteins EHD1 and EHD2 interact with fer-1-like-5 (Fer1L5) and mediate myoblast fusion. J Biol Chem. 2011; 286:7379–7388. [PubMed: 21177873]
35. Doherty KR, Demonbreun AR, Wallace GQ, Cave A, Posey AD, Heretis K, Pytel P, McNally EM. The endocytic recycling protein EHD2 interacts with myoferlin to regulate myoblast fusion. J Biol Chem. 2008; 283:20252–20260. [PubMed: 18502764]

36. Cypher LR, Bielecki TA, Huang L, An W, Iseka F, Tom E, Storck MD, Hoppe AD, Band V, Band H. CSF-1 receptor signalling is governed by pre-requisite EHD1 mediated receptor display on the macrophage cell surface. Cell Signal. 2016; 28:1325–1335. [PubMed: 27224507]
37. Bhattacharyya S, Rainey MA, Arya P, Dutta S, George M, Storck MD, McComb RD, Muirhead D, Todd GL, Gould K, Datta K, Gelineau-van Waes J, Band V, Band H. Endocytic recycling protein EHD1 regulates primary cilia morphogenesis and SHH signaling during neural tube development. Sci Rep. 2016; 6:20727. [PubMed: 26884322]
38. Arya P, Rainey MA, Bhattacharyya S, Mohapatra BC, George M, Kuracha MR, Storck MD, Band V, Govindarajan V, Band H. The endocytic recycling regulatory protein EHD1 Is required for ocular lens development. Dev Biol. 2015; 408:41–55. [PubMed: 26455409]
39. Naslavsky N, Boehm M, Backlund PS Jr, Caplan S. Rabenosyn-5 and EHD1 interact and sequentially regulate protein recycling to the plasma membrane. Mol Biol Cell. 2004; 15:2410–2422. [PubMed: 15020713]
40. Naslavsky N, Rahajeng J, Sharma M, Jovic M, Caplan S. Interactions between EHD proteins and Rab11-FIP2: a role for EHD3 in early endosomal transport. Mol Biol Cell. 2006; 17:163–177. [PubMed: 16251358]
41. Rotem-Yehudar R, Galperin E, Horowitz M. Association of insulin-like growth factor 1 receptor with EHD1 and SNAP29. J Biol Chem. 2001; 276:33054–33060. [PubMed: 11423532]
42. Lu Q, Insinna C, Ott C, Stauffer J, Pintado PA, Rahajeng J, Baxa U, Walia V, Cuenca A, Hwang YS, Daar IO, Lopes S, Lippincott-Schwartz J, Jackson PK, Caplan S, Westlake CJ. Early steps in primary cilium assembly require EHD1/EHD3-dependent ciliary vesicle formation. Nat Cell Biol. 2015; 17:531.
43. Braun A, Pinyol R, Dahlhaus R, Koch D, Fonarev P, Grant BD, Kessels MM, Qualmann B. EHD proteins associate with syndapin I and II and such interactions play a crucial role in endosomal recycling. Mol Biol Cell. 2005; 16:3642–3658. [PubMed: 15930129]
44. Giridharan SS, Cai B, Vitale N, Naslavsky N, Caplan S. Cooperation of MICAL-L1, syndapin2, and phosphatidic acid in tubular recycling endosome biogenesis. Mol Biol Cell. 2013; 24:1776–90. S1–15. [PubMed: 23596323]
45. Sharma M, Naslavsky N, Caplan S. A role for EHD4 in the regulation of early endosomal transport. Traffic. 2008; 9:995–1018. [PubMed: 18331452]
46. Finetti F, Patrussi L, Masi G, Onnis A, Galgano D, Lucherini OM, Pazour GJ, Baldari CT. Specific recycling receptors are targeted to the immune synapse by the intraflagellar transport system. J Cell Sci. 2014; 127:1924–1937. [PubMed: 24554435]
47. Finetti F, Patrussi L, Galgano D, Cassioli C, Perinetti G, Pazour GJ, Baldari CT. The small GTPase Rab8 interacts with VAMP-3 to regulate the delivery of recycling T-cell receptors to the immune synapse. J Cell Sci. 2015; 128:2541–2552. [PubMed: 26034069]
48. Patino-Lopez G, Dong X, Ben-Aissa K, Bernot KM, Itoh T, Fukuda M, Kruhlak MJ, Samelson LE, Shaw S. Rab35 and its GAP EPI64C in T cells regulate receptor recycling and immunological synapse formation. J Biol Chem. 2008; 283:18323–18330. [PubMed: 18450757]
49. Rainey MA, George M, Ying G, Akakura R, Burgess DJ, Siefker E, Bargar T, Doglio L, Crawford SE, Todd GL, Govindarajan V, Hess RA, Band V, Naramura M, Band H. The endocytic recycling regulator EHD1 is essential for spermatogenesis and male fertility in mice. BMC Dev Biol. 2010; 10 37-213X-10-37.
50. Kamala T. An optimized immunomagnetic bead-based negative selection protocol for CD4 T-cell isolation from mouse lymph nodes and spleen. Scand J Immunol. 2008; 67:285–294. [PubMed: 18261040]
51. Carrasco YR, Navarro MN, Toribio ML. A role for the cytoplasmic tail of the pre-T cell receptor (TCR) alpha chain in promoting constitutive internalization and degradation of the pre-TCR. J Biol Chem. 2003; 278:14507–14513. [PubMed: 12473666]
52. Dietrich J, Menne C, Lauritsen JP, von Essen M, Rasmussen AB, Odum N, Geisler C. Ligand-induced TCR down-regulation is not dependent on constitutive TCR cycling. J Immunol. 2002; 168:5434–5440. [PubMed: 12023336]
53. Osborne DG, Piotrowski JT, Dick CJ, Zhang JS, Billadeau DD. SNX17 affects T cell activation by regulating TCR and integrin recycling. J Immunol. 2015; 194:4555–4566. [PubMed: 25825439]

54. Sullivan BM, Coscoy L. Downregulation of the T-cell receptor complex and impairment of T-cell activation by human herpesvirus 6 u24 protein. J Virol. 2008; 82:602–608. [PubMed: 17977973]
55. Bettelli E, Pagany M, Weiner HL, Linington C, Sobel RA, Kuchroo VK. Myelin oligodendrocyte glycoprotein-specific T cell receptor transgenic mice develop spontaneous autoimmune optic neuritis. J Exp Med. 2003; 197:1073–1081. [PubMed: 12732654]
56. George M, Rainey MA, Naramura M, Ying G, Harms DW, Vitaterna MH, Doglio L, Crawford SE, Hess RA, Band V, Band H. Ehd4 is required to attain normal prepubertal testis size but dispensable for fertility in male mice. Genesis. 2010; 48:328–342. [PubMed: 20213691]
57. George M, Rainey MA, Naramura M, Foster KW, Holzapfel MS, Willoughby LL, Ying G, Goswami RM, Gurumurthy CB, Band V, Satchell SC, Band H. Renal thrombotic microangiopathy in mice with combined deletion of endocytic recycling regulators EHD3 and EHD4. PLoS One. 2011; 6:e17838. [PubMed: 21408024]
58. Liu G, Li Z, Wei Y, Lin Y, Yang C, Liu T. Direct detection of FoxP3 expression in thymic double-negative CD4-CD8- cells by flow cytometry. Sci Rep. 2014; 4:5781. [PubMed: 25060864]
59. Dashtsoodol N, Watarai H, Sakata S, Taniguchi M. Identification of CD4(−)CD8(−) double-negative natural killer T cell precursors in the thymus. PLoS One. 2008; 3:e3688. [PubMed: 18997862]
60. Wang Y, Becker D, Vass T, White J, Marrack P, Kappler JW. A conserved CXXC motif in CD3epsilon is critical for T cell development and TCR signaling. PLoS Biol. 2009; 7:e1000253. [PubMed: 19956738]
61. Malek TR, Yu A, Scibelli P, Lichtenheld MG, Codias EK. Broad programming by IL-2 receptor signaling for extended growth to multiple cytokines and functional maturation of antigen-activated T cells. J Immunol. 2001; 166:1675–1683. [PubMed: 11160210]
62. Boyman O, Sprent J. The role of interleukin-2 during homeostasis and activation of the immune system. Nat Rev Immunol. 2012; 12:180–190. [PubMed: 22343569]
63. von Essen M, Bonefeld CM, Siersma V, Rasmussen AB, Lauritsen JP, Nielsen BL, Geisler C. Constitutive and ligand-induced TCR degradation. J Immunol. 2004; 173:384–393. [PubMed: 15210797]
64. Qureshi OS, Kaur S, Hou TZ, Jeffery LE, Poulter NS, Briggs Z, Kenefeck R, Willox AK, Royle SJ, Rappoport JZ, Sansom DM. Constitutive clathrin-mediated endocytosis of CTLA-4 persists during T cell activation. J Biol Chem. 2012; 287:9429–9440. [PubMed: 22262842]
65. Valk E, Rudd CE, Schneider H. CTLA-4 trafficking and surface expression. Trends Immunol. 2008; 29:272–279. [PubMed: 18468488]
66. Andres PG, Howland KC, Dresnek D, Edmondson S, Abbas AK, Krummel MF. CD28 signals in the immature immunological synapse. J Immunol. 2004; 172:5880–5886. [PubMed: 15128767]
67. Daniels MA, Teixeiro E. TCR Signaling in T Cell Memory. Front Immunol. 2015; 6:617. [PubMed: 26697013]
68. Cantrell D. T cell antigen receptor signal transduction pathways. Annu Rev Immunol. 1996; 14:259–274. [PubMed: 8717515]
69. Surh CD, Sprent J. Homeostasis of naive and memory T cells. Immunity. 2008; 29:848–862. [PubMed: 19100699]
70. Furtado GC, Marcondes MC, Latkowski JA, Tsai J, Wensky A, Lafaille JJ. Swift entry of myelin-specific T lymphocytes into the central nervous system in spontaneous autoimmune encephalomyelitis. J Immunol. 2008; 181:4648–4655. [PubMed: 18802067]
71. O'Connor RA, Prendergast CT, Sabatos CA, Lau CW, Leech MD, Wraith DC, Anderton SM. Cutting edge: Th1 cells facilitate the entry of Th17 cells to the central nervous system during experimental autoimmune encephalomyelitis. J Immunol. 2008; 181:3750–3754. [PubMed: 18768826]
72. Soares H, Henriques R, Sachse M, Ventimiglia L, Alonso MA, Zimmer C, Thoulouze MI, Alcover A. Regulated vesicle fusion generates signaling nanoterritories that control T cell activation at the immunological synapse. J Exp Med. 2013; 210:2415–2433. [PubMed: 24101378]
73. Finetti F, Paccani SR, Riparbelli MG, Giacomello E, Perinetti G, Pazour GJ, Rosenbaum JL, Baldari CT. Intraflagellar transport is required for polarized recycling of the TCR/CD3 complex to the immune synapse. Nat Cell Biol. 2009; 11:1332–1339. [PubMed: 19855387]

74. Yuan X, Garrett-Sinha LA, Sarkar D, Yang S. Deletion of IFT20 in early stage T lymphocyte differentiation inhibits the development of collagen-induced arthritis. Bone Res. 2014; 2:14038. [PubMed: 26097753]

75. Piotrowski JT, Gomez TS, Schoon RA, Mangalam AK, Billadeau DD. WASH knockout T cells demonstrate defective receptor trafficking, proliferation, and effector function. Mol Cell Biol. 2013; 33:958–973. [PubMed: 23275443]

76. Jia D, Gomez TS, Metlagel Z, Umetani J, Otwinowski Z, Rosen MK, Billadeau DD. WASH and WAVE actin regulators of the Wiskott-Aldrich syndrome protein (WASP) family are controlled by analogous structurally related complexes. Proc Natl Acad Sci U S A. 2010; 107:10442–10447. [PubMed: 20498093]

77. Gautreau A, Oguievetskaia K, Ungermann C. Function and regulation of the endosomal fusion and fission machineries. Cold Spring Harb Perspect Biol. 2014; 6doi: 10.1101/cshperspect.a016832

78. Seaman MN. The retromer complex - endosomal protein recycling and beyond. J Cell Sci. 2012; 125:4693–4702. [PubMed: 23148298]

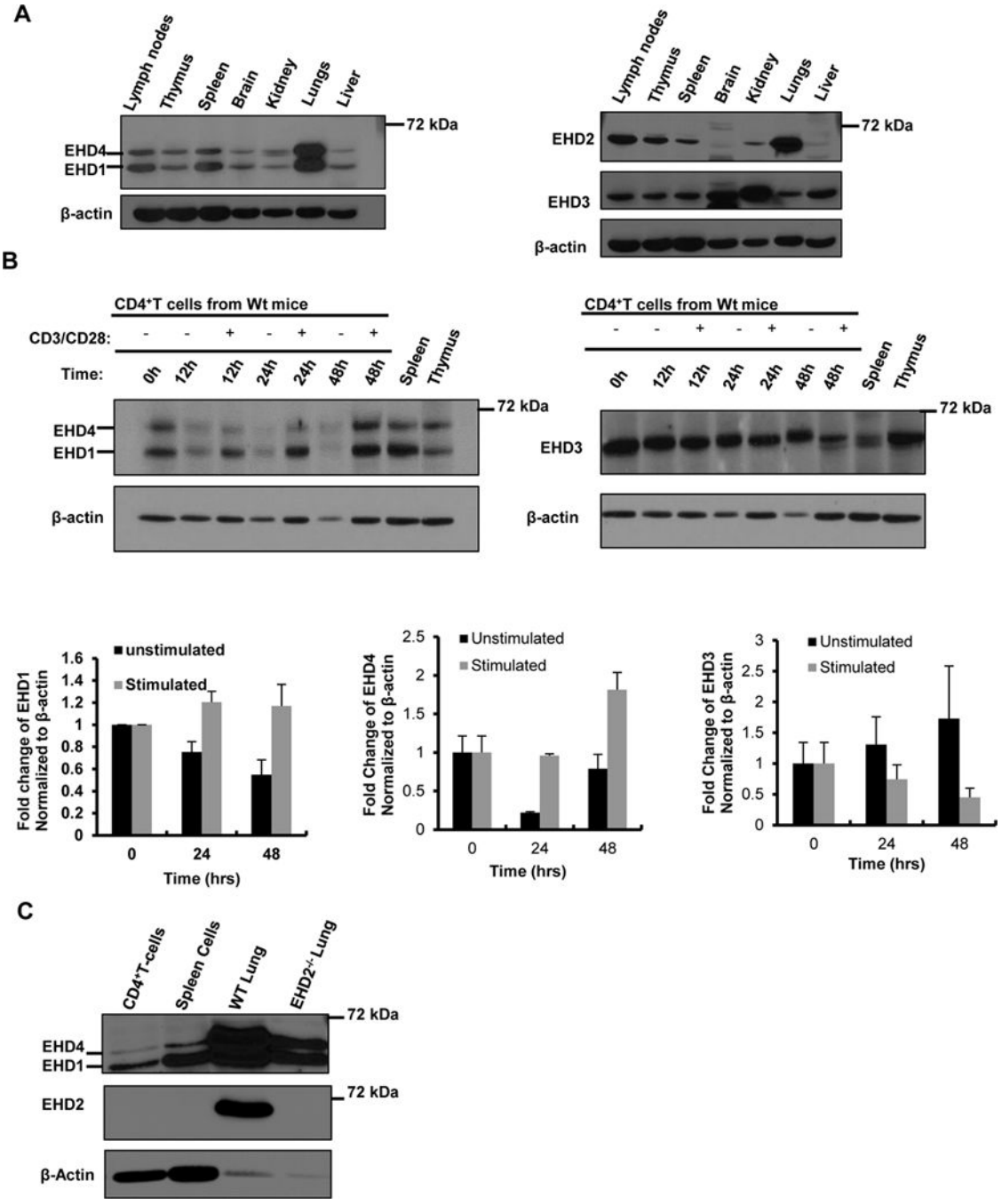

Figure 1. Expression of EHDs in lymphoid tissues and isolated CD4$^+$ T-cells

A) Lymphoid tissues express all EHD proteins. One membrane (left) was probed with an antibody recognizing both EHD1 and EHD4, and a second one (right) probed for EHD3 followed by re-probing for EHD2. **B)** EHD protein expression in CD4$^+$ T-cells and changes in expression following activation are shown. Shown is a representative blot of more than 3 independent experiments. CD4$^+$ T cells were isolated from pooled LN cells of at least 5 mice per group for each experiment (however, quantification shown is of EHD protein levels for the time points used in all the repeats, normalized to β-actin, and plotted as the mean ±

SEM of N=2). **C)** Lysate of $CD4^+$ T-cells from WT spleen was loaded together with lysates from WT spleen cells, WT lung and $EHD2^{-/-}$ lung as controls. The membrane was probed for EHD1 and EHD4 and re-probed for EHD2 level; β-actin was used as loading control (N=3).

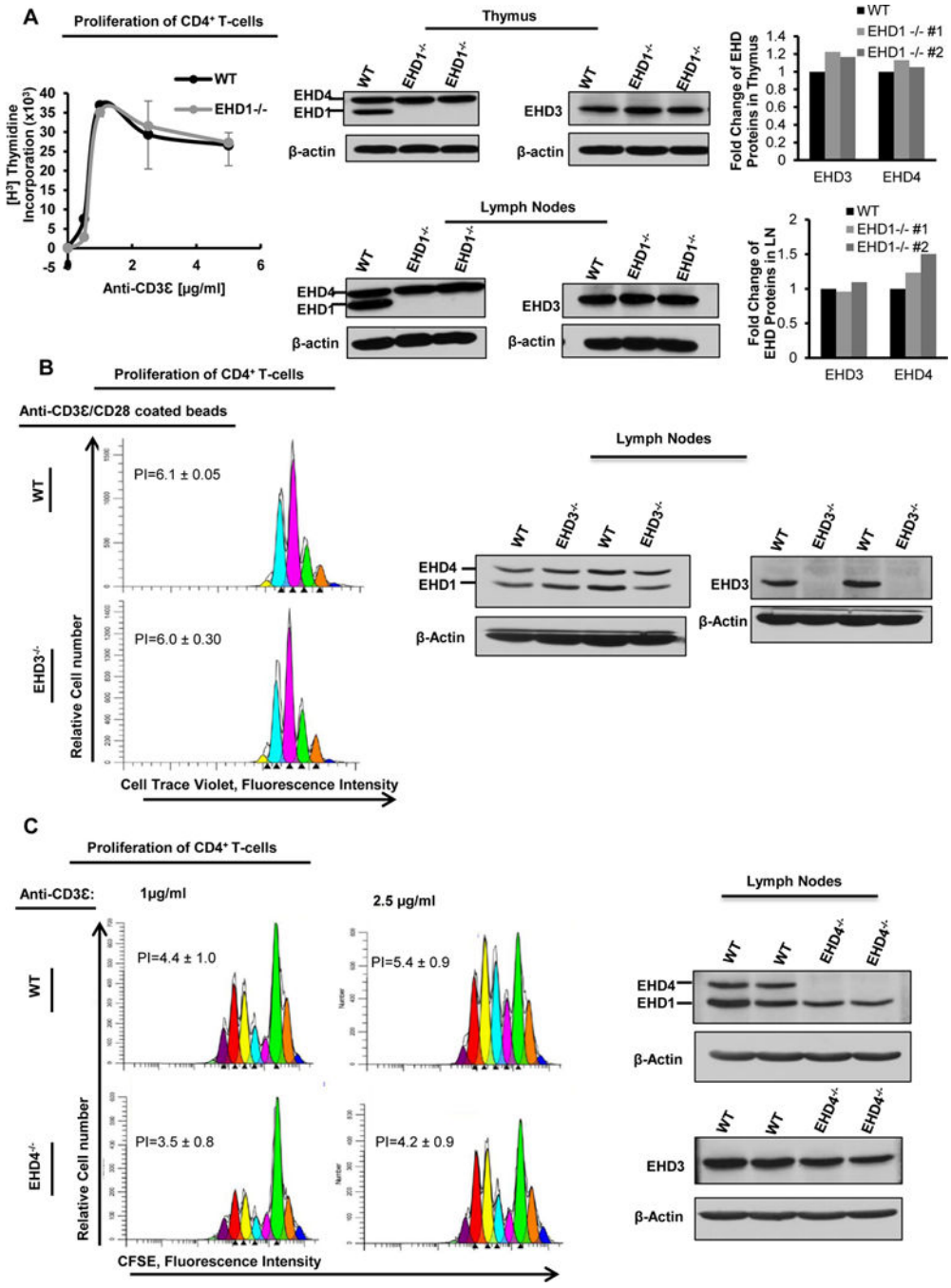

Figure 2. Potential redundancy among EHD proteins

A) Left, freshly isolated $CD4^+$ T-cells from $EHD1^{-/-}$ and WT littermate mice were stimulated with anti-CD3Ɛ and anti CD28 for 72 hrs and were ^3H-thymidine was added for the last 6 hrs of incubation. A representative figure of 3 independent experiments is shown. Middle, expression of EHD proteins in lymphoid organs from one WT and two $EHD1^{-/-}$ mice. Tissue lysates from the shown organs were resolved on a 10% SDS-PAGE gel and immunoblotted for EHD proteins. Right, quantification of each blot. **B)** Left, lymph node cells from WT and $EHD3^{-/-}$ mice were stained with cell-trace violet, then stimulated with

anti-CD3Ɛ/CD28-coated beads for 3 days. Cells were stained with anti-CD4 to assess the proliferation profile of $CD4^+$ T-cells. FACS data modelled using ModFit software is shown. PI = proliferation index ± SEM of N = 2. Right, western blot of lymph node lysates showing deletion of EHD3 in $EHD3^{-/-}$ mice and lack of impact on EHD1/4 levels. **C)** Left, lymph nodes cells from WT and $EHD4^{-/-}$ mice were stained with CFSE and stimulated with anti-CD3Ɛ (1 μg/ml or 2.5μg/ml) together with 1μg/ml anti-CD28 for 3 days. Cells were stained with anti-CD4 to assess the proliferation profile of $CD4^+$ T-cells. FACS data modelled using ModFit software is shown. PI = proliferation index ± SEM of N = 3. Right, western blot of lymph node lysates showing deletion of EHD4 in $EHD4^{-/-}$ mice.

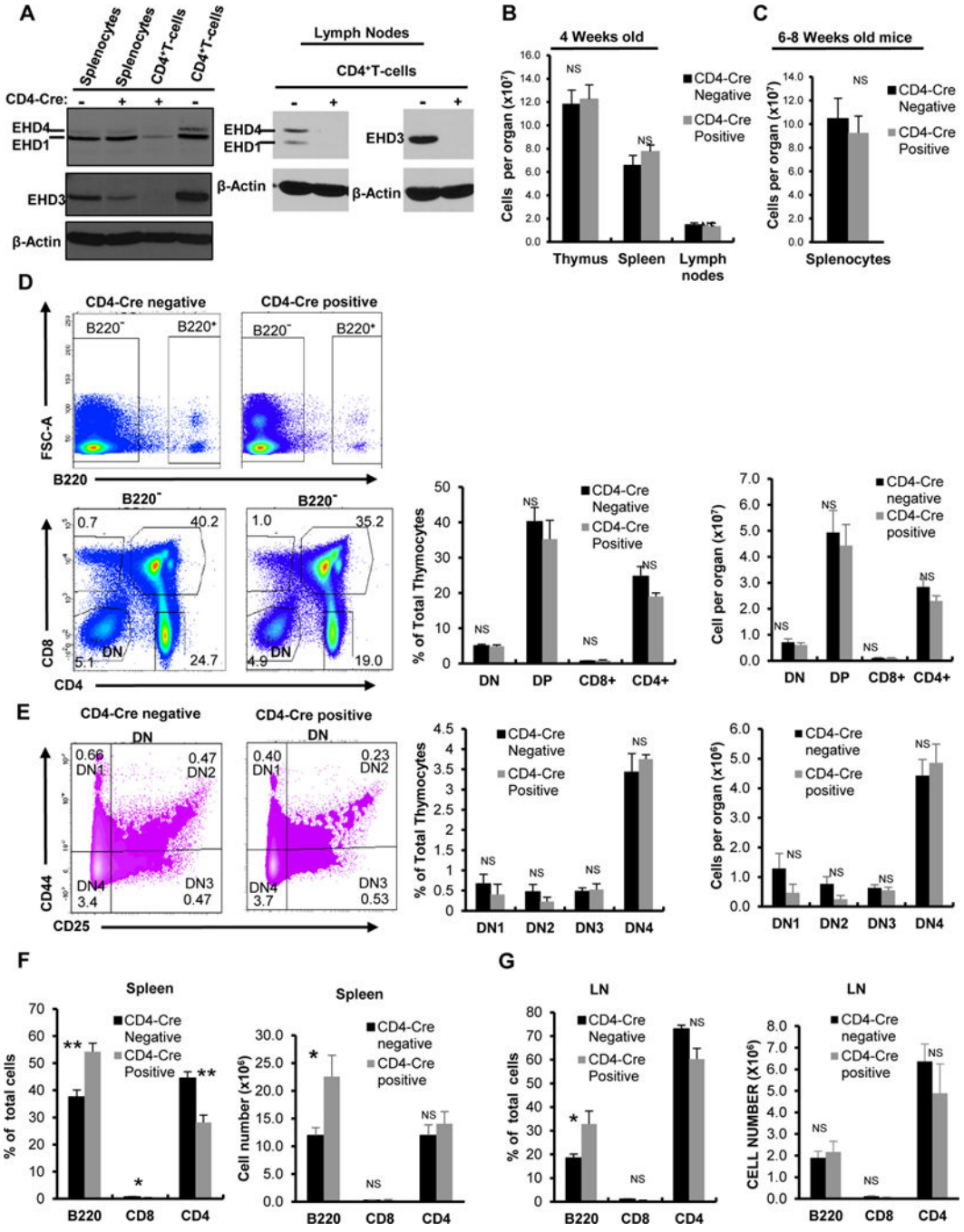

Figure 3. CD4-Cre mediated conditional deletion of EHD 1, 3 and 4 does not impact thymic T-cell development but leads to a relative decrease in CD4$^+$ T-cells in secondary lymphoid tissues

A) Western Blot verification of EHD1/3/4 deletions is shown. Lysates of freshly isolated splenocytes from the same mice before T-cell expansion were used as controls. A representative blot of N=6 is shown. **B & C)** There was no change in the absolute number of cells in the different lymphoid tissues of CD4-Cre$^+$ mice. In **B)** cell numbers were counted in single cell preparations of the indicated lymphoid organs of 4-week-old CD4-Cre$^+$ and CD4-Cre$^-$ (control) mice; N=5. In **C**, the total spleen cell numbers from adult (6–8 weeks

old) mice are shown; N=5. **D & E)** Analysis of thymic developmental stages in CD4-Cre^{+} and CD4-Cre^{-} mice are shown. **D)** Left shows representative FACS plots with gating strategies used for analysis of cell subsets and developmental stages in thymocytes of 4-week-old mice. The numbers in quadrants represent the mean percentage of total thymocytes. Right shows quantification of left panels. **E)** left shows FACS plots with gating strategies and right shows quantification of relative percentages of cell subsets or cell numbers as in **D)**, N=4. **F & G)** Reduced percentages of T-cells in the spleen and increased percentages of B cells in the spleen and LN are shown. Spleen **(F)** and LN cells **(G)** from 4-week-old CD4-Cre^{+} and CD4-Cre^{-} mice were analyzed by FACS for markers of B cells (B220^{+}), CD8^{+} T-cells and CD4^{+} T-cells (N=4). Total cell numbers were calculated by multiplying the total live cell counts with the percentage of each subset. All values plotted as the mean ± SEM for indicated sample size. *, $p<0.05$; **, $p<0.01$.

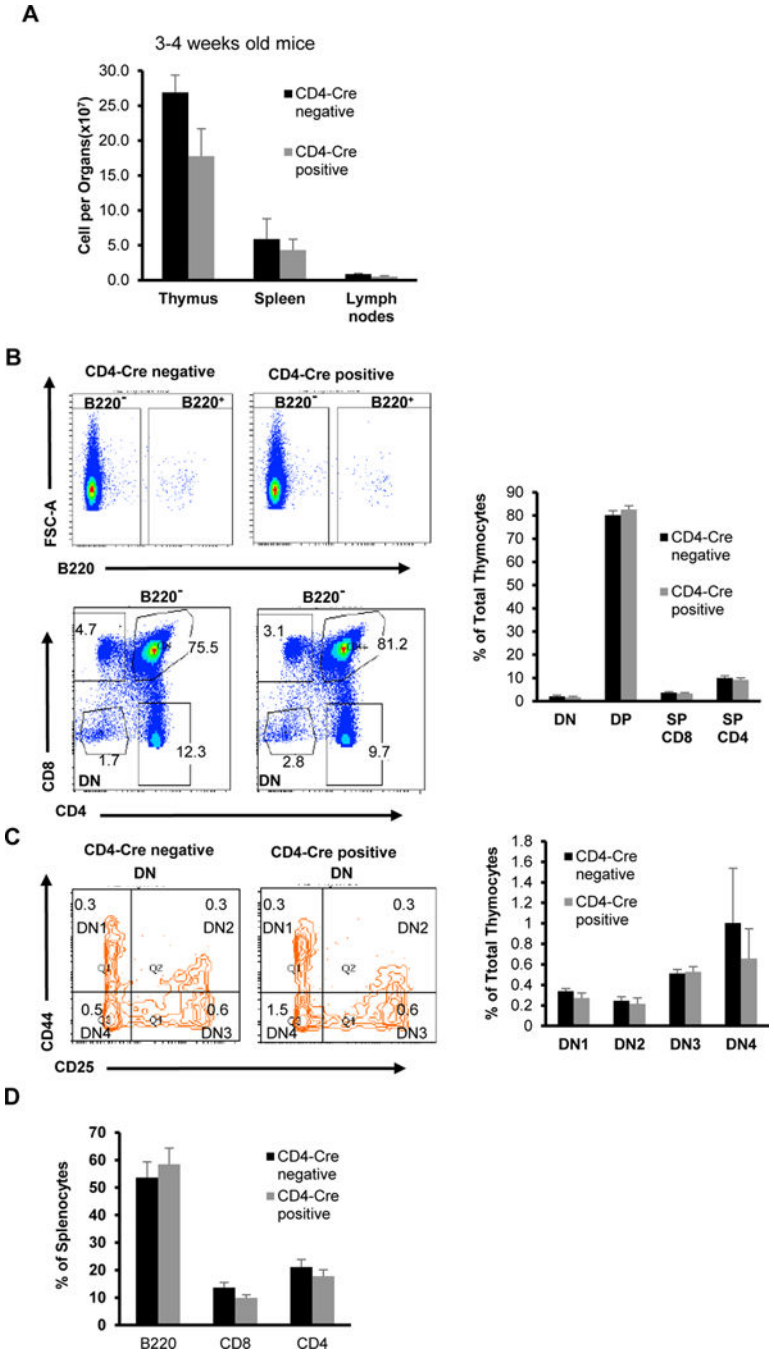

Figure 4. CD4-Cre mediated conditional deletion of EHD 1, 3 and 4 does not impact thymic T-cell development in non-TCR-transgenic mice

A) Cell numbers were counted in single cell preparations of the indicated lymphoid organs of 3–4-week-old CD4-Cre^{+} and CD4-Cre^{-} (control) mice; N=4. **B & C)** Analysis of thymic developmental stages in CD4-Cre^{+} and CD4-Cre^{-} mice are shown. **B)** The left panels show representative FACS plots with gating strategies used for analysis of cell subsets and developmental stages in thymocytes of 3–4-week-old mice. The numbers in quadrants represent the mean percentage of total thymocytes. The right panels show quantification of

results shown in left panels. **C)** The left panel show FACS plots with gating strategies for the DN stage and the right panel shows the quantification of relative percentages of cell subsets, N=4. **D)** Spleens from 3–4-week-old CD4-Cre^{+} and CD4-Cre^{-} mice were analyzed by FACS for markers of B cells (B220^{+}), CD8^{+} T-cells and CD4^{+} T-cells (N=4). All values are plotted as mean ± SEM for the indicated sample size.

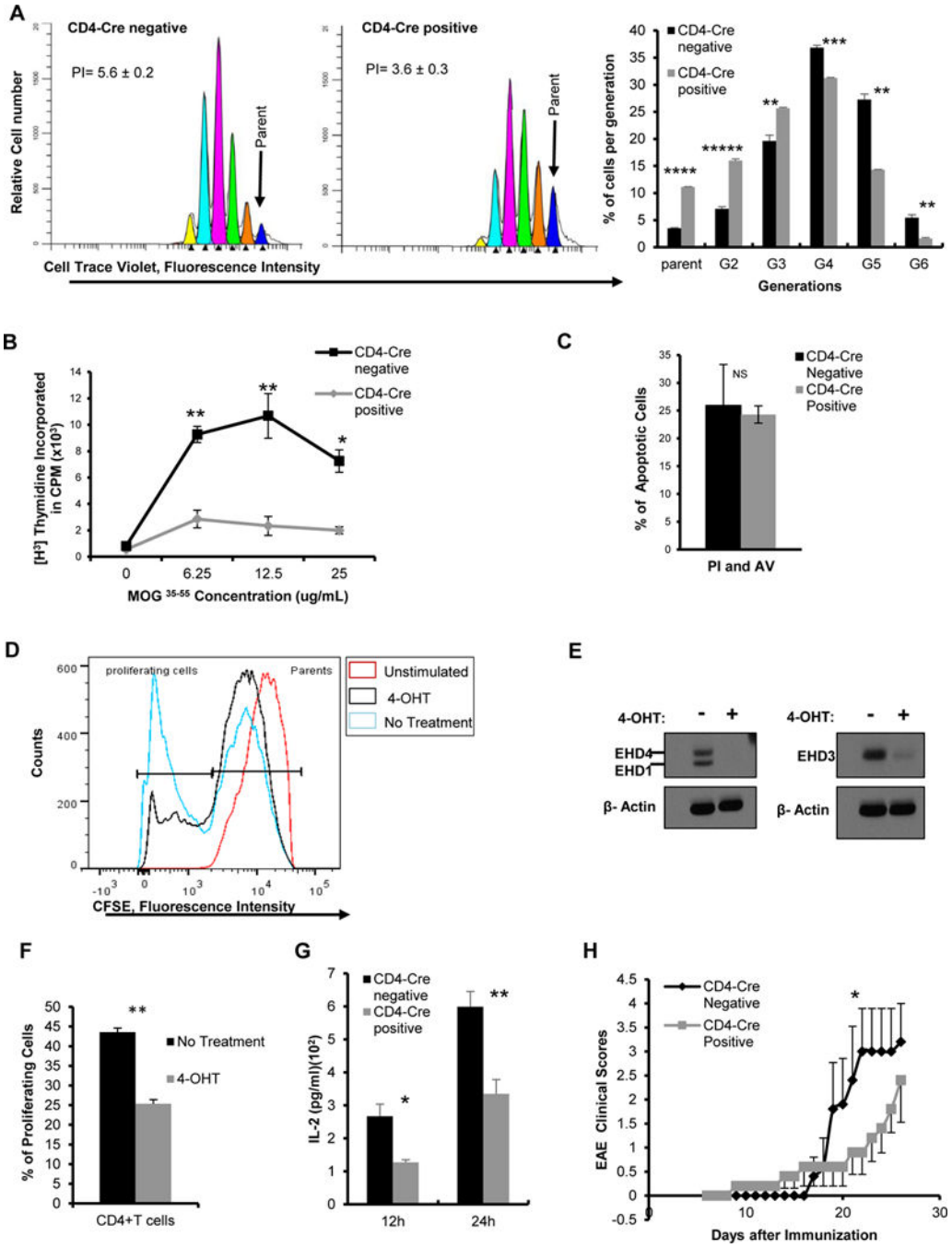

Figure 5. Conditional deletion of EHD 1, 3 and 4 in T-cells leads to reduced cell proliferation and IL-2 secretion

A) A reduced proliferation by Cell-Trace Violet dye dilution assay is shown. Successive cell divisions were modeled with ModFit LT software and are shown as peaks of different colors. The figure is a representative of N=3. The mean percentages of cells at successive divisions are shown on the right as a histogram. The proliferation index (PI) shown on top is the mean ± SEM of N=3. *, p<0.05; **, p<0.01; ***, p<0.001; ****, p<0.0001; *****, p<0.00001. **B)** Reduced proliferation seen by ^{3}H-thymidine incorporation assay is shown. Shown is a

representative figure of N=2. **C)** Cells were stimulated as previously mentioned for the proliferation assays and stained with propidium iodide (PI) and anti-Annexin V antibody followed by FACS analysis for relative proportions of PI^+/Annexin V^+ apoptotic cells. Values represent mean ± SEM. of N=2 (NS, not significant). **D)** Spleen cells from *EHD1*$^{fl/fl}$*; EHD3*$^{fl/fl}$*; EHD4*$^{fl/fl}$*; Cre*^{ERT2}*; 2D2Tcr* mice were stimulated with anti-CD3/CD28 in the presence or absence of 4-OH-tamoxifen (4-OHT) for four days to derive in vitro EHD 1/3/4-deleted T-cells vs. their WT controls. Cells were washed, loaded with CFSE dye and re-stimulated with anti-CD3/CD28 for 72 hrs. Cells were as in **A)**. Shown is a representative figure of N=2. **E)** Western blot used to show depletion of EHD 1/3/4 in tamoxifen-treated T-cells. **F)** Quantification of the percentage of proliferating cells from the data shown in **D)**. **G)** Reduced IL-2 secretion is shown. Values represent mean ± SEM, N=4, * $p<0.05$, ** $p<0.01$). **H)** There was a reduced severity of EAE in CD4-Cre^+ mice. The plotted values are the composite mean scores ± SEM, N=5 in each group, *, $p<0.05$. Clinical scores were recorded as described in Methods.

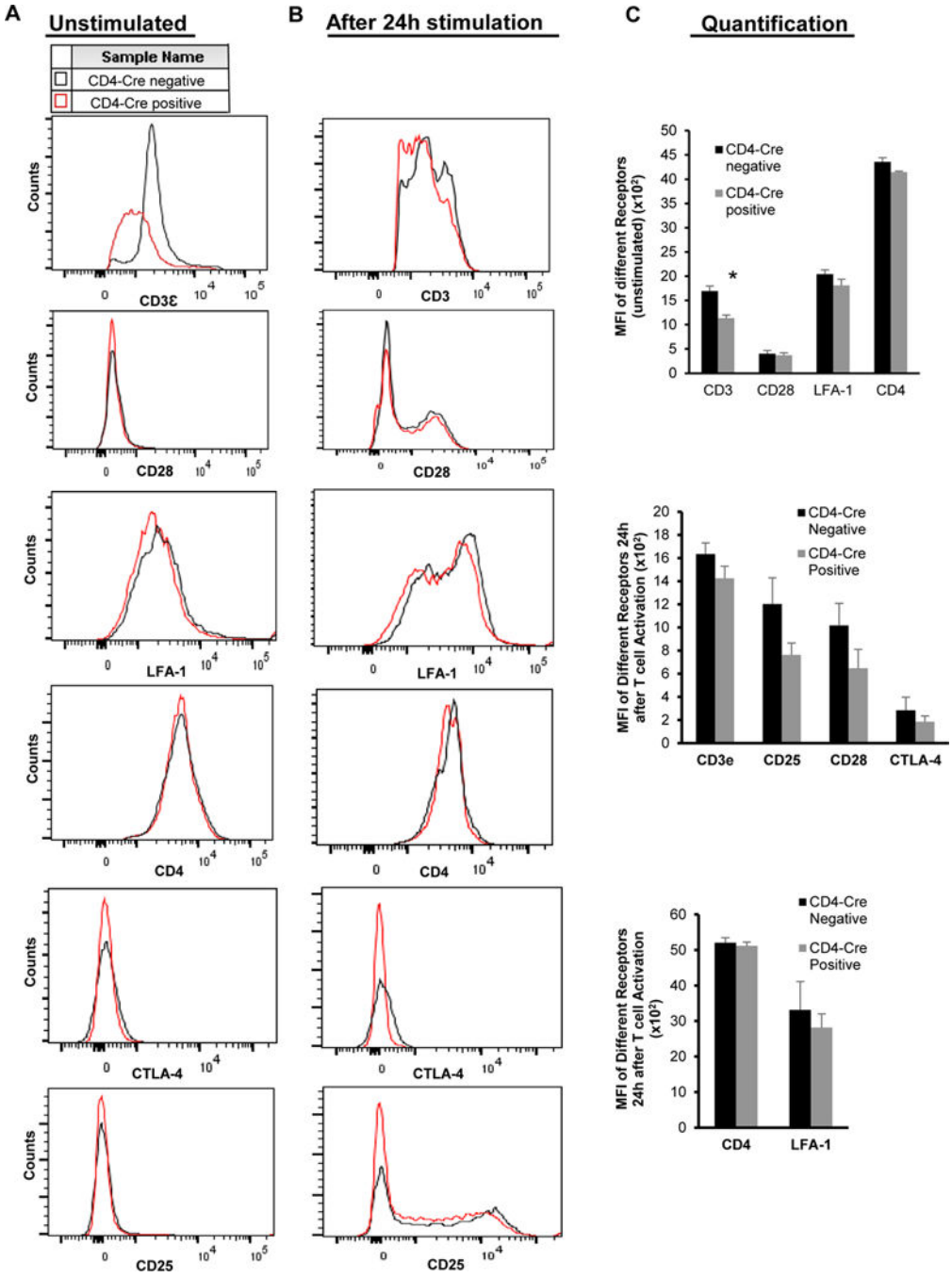

Figure 6. Conditional deletion of EHD 1, 3 and 4 leads to impairment of basal surface level of TCR-CD3

A) Spleen cells were stained with directly conjugated antibodies for indicated receptors and were gated on $CD3^+$ T cells to analyze the median intensity level (MFI) of each receptor. Shown is a representative histogram of the surface levels of TCR-CD3 (anti-CD3ε), CD28, CD4, CD25, CTLA-4 and LFA1 at steady-state. **B)** A representative histogram of the surface levels of TCR-CD3, CD28, CD4, CD25, CTLA-4 and LFA1 after 24h stimulation with the

MOG peptide is shown. **C)** The MFI values were plotted as mean ± SEM of N=3 (*, $p<0.05$).

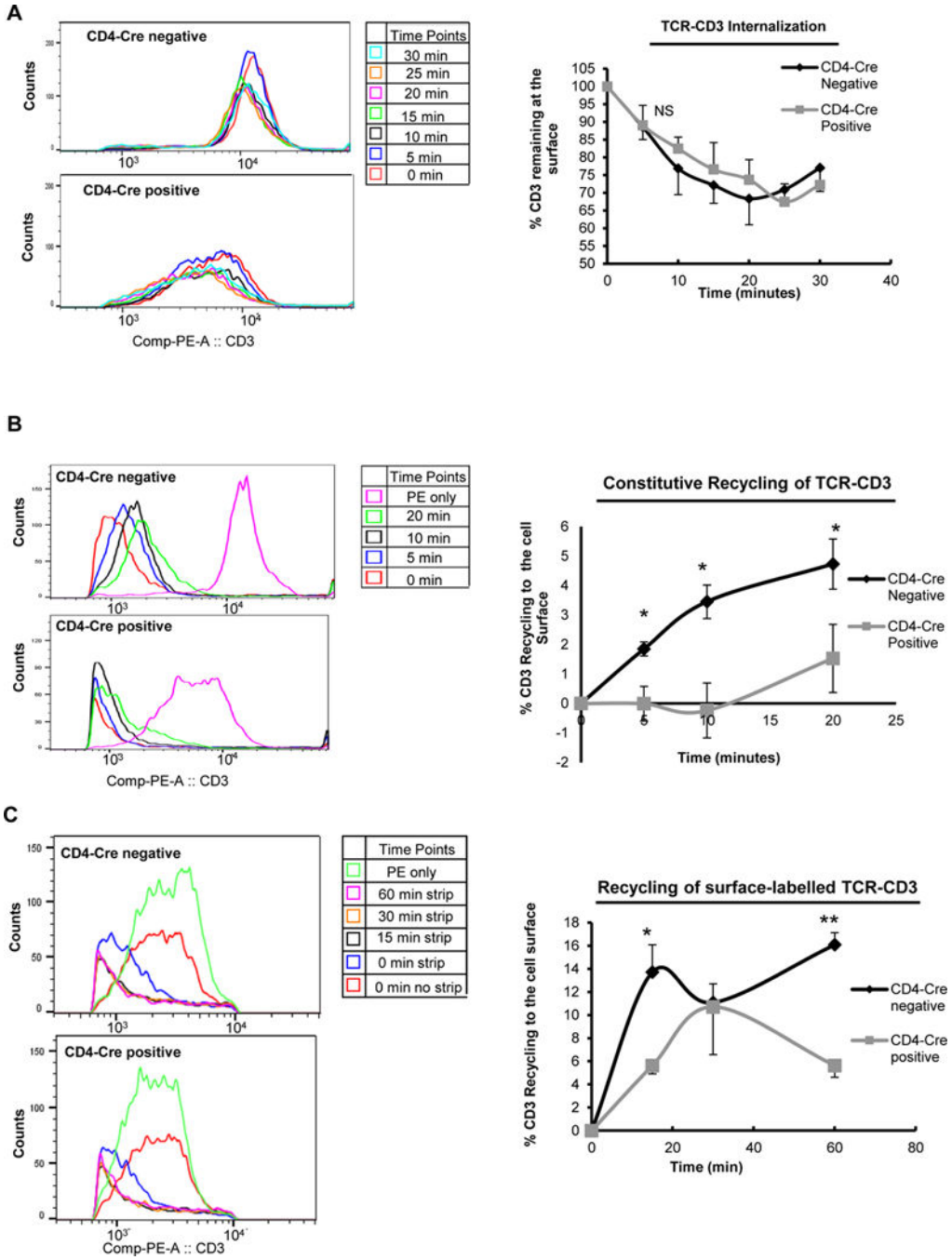

Figure 7. Conditional deletion of EHD 1, 3 and 4 leads to impairment of basal recycling of TCR-CD3 from endocytic compartments to the cell surface

A) A relatively intact basal TCR-CD3 internalization is shown. N=3; NS, not significant. A representative histogram of the MFIs of TCR-CD3 internalization is shown on the left. **B)** Reduced recycling of pre-existing endosomal TCR-CD3 is shown. The data represent mean ± SEM. of N=4 (*p<0.05). A representative histogram of the MFI of TCR-CD3 recycling is shown on the left. **C)** Recycling of the labelled cell surface TCR-CD3 is shown. Cells were analyzed by FACS and MFI values used to quantify the proportion of internalized receptors

that were still intracellular (acid wash-resistant fraction) and the percent of recycling was calculated as described in Methods. Values plotted are mean ± SEM of N=4. *, $p<0.05$, **, $p<0.01$. A representative histogram of the MFIs of TCR-CD3 recycling is shown on the left.

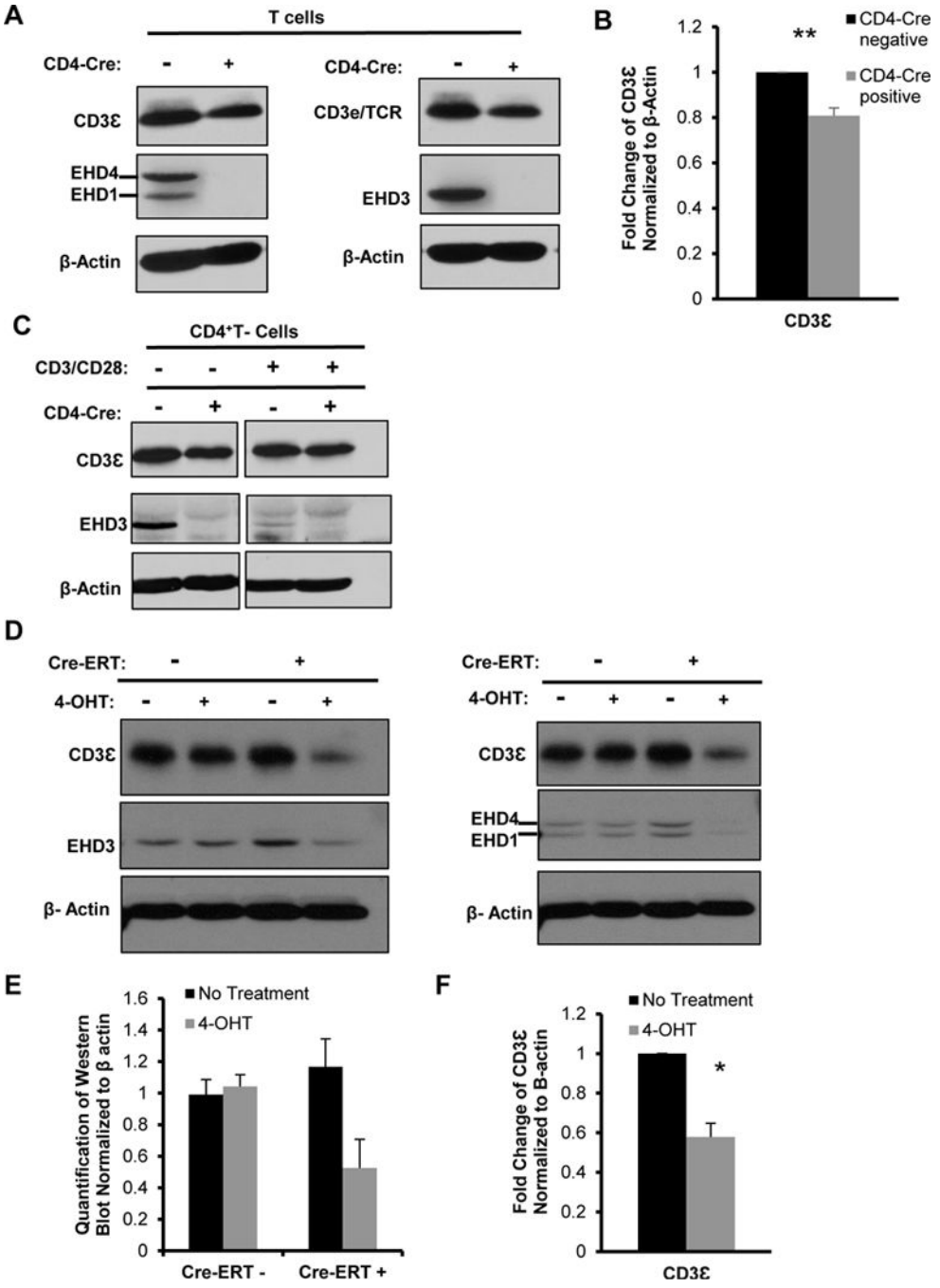

Figure 8. Conditional deletion of EHD 1, 3 and 4 leads to a reduced level of the CD3ε component of TCR-CD3

A) Expanded T-cells from LN of CD4-Cre^{-} or CD4-Cre^{+} mice probed for CD3Ɛ and either EHD1/4 or EHD3 proteins**. B)** Quantification of CD3Ɛ signals. Values plotted are mean ± SEM. of N=5. **C)** Lysates of freshly-isolated CD4^{+} T-cells from CD4-Cre positive and CD4-Cre negative mice before and after 72h anti-CD3/anti-CD28 activation were western blotted for EHD3 and CD3Ɛ levels. β-actin was used as loading control. **D)** LN cells from *EHD1$^{fl/fl}$; EHD3$^{fl/fl}$; EHD4$^{fl/fl}$; Cre^{ERT2}; 2D2-Tcr* or *EHD1$^{fl/fl}$; EHD3$^{fl/fl}$; EHD4$^{fl/fl}$;*

2D2Tcr (control) mice were stimulated with anti-CD3/CD28 for four days in the presence (+) or absence (−) of 4-OHT. Lysate from equal numbers of cells were loaded in each lane. Western blot was carried out as in B. Shown is a representative blot run in duplicate. **E)** Quantification of CD3ε signals for blot shown in **D**. **F)** Quantification of CD3ε signals for Cre-ERT^{+} T-cells. Values plotted are mean ± SEM of N=3 *p<0.05, **P<0.01.

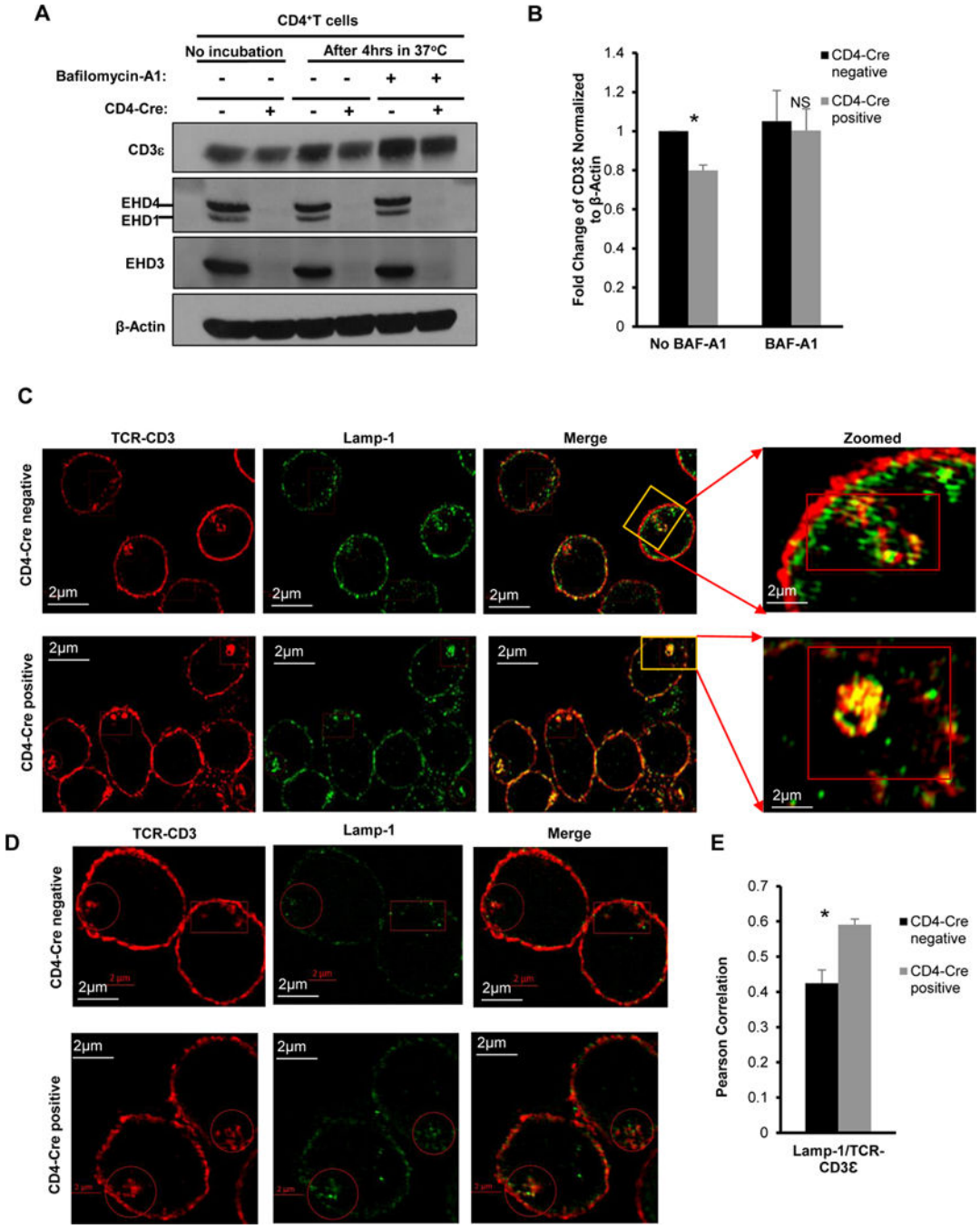

Figure 9. Conditional deletion of EHD 1, 3 and 4 leads to lysosomal degradation of TCR-CD3

A) T-cells expanded from LN of CD4-Cre^{-} or CD4-Cre^{+} mice (7–8 days) were washed and treated with (+) or without (−) 100 nM Bafilomycin-A1 for 4 h at 37°C. Lysate from equal numbers of cells was run, probed for CD3ε and EHD1/4 and re-probed for EHD3, with β-actin as a loading control. A representative blot is shown. **B)** Quantification from data exhibited in **A** are shown here. Values plotted are mean ± SEM of N=3. **C)** Expanded T-cells from LN of CD4-Cre^{-} or CD4-Cre^{+} mice were treated with Bafilomycin-A1 as in **A** and stained with anti-CD3ε (Red) and anti-LAMP1 (Green) antibodies followed by confocal

imaging. Shown is a representative image of N=3. Scale bar = 2 μm. **D)** Anti-CD3/anti-CD28-expanded T-cells from LN of CD4-Cre^{-} or CD4-Cre^{+} mice that were not treated with Bafilomycin-A1 were stained with anti-CD3ε (Red) and anti-LAMP1 (Green) antibodies followed by confocal imaging. Shown is a representative image of N=3. The red boxes indicate the intracellular pools of CD3ε that were used to determine the Pearson correlation coefficients (from analyses of >50 cells per group) as an indicator of the extent of CD3ε/LAMP1 co-localization, which is shown in **E)**. Values are mean ± SEM, *$p<0.05$.